Linking eutrophication to carbon dioxide and methane emissions from exposed mangrove soils along an urban gradient

Glenda C Barroso, Gwenaël Abril, Wilson Machado, Rodrigo C Abuchacra, Roberta B Peixoto, Marcelo Bernardes, Gabriela S Marques, Christian J Sanders, Gabriela B Oliveira, Silvio R Oliveira Filho, et al.

▶ **To cite this version:**

Glenda C Barroso, Gwenaël Abril, Wilson Machado, Rodrigo C Abuchacra, Roberta B Peixoto, et al.. Linking eutrophication to carbon dioxide and methane emissions from exposed mangrove soils along an urban gradient. Science of the Total Environment, 2022, 850, pp.157988. 10.1016/j.scitotenv.2022.157988 . hal-03813858

HAL Id: hal-03813858
https://cnrs.hal.science/hal-03813858

Submitted on 13 Oct 2022

HAL is a multi-disciplinary open access archive for the deposit and dissemination of scientific research documents, whether they are published or not. The documents may come from teaching and research institutions in France or abroad, or from public or private research centers.

L'archive ouverte pluridisciplinaire **HAL**, est destinée au dépôt et à la diffusion de documents scientifiques de niveau recherche, publiés ou non, émanant des établissements d'enseignement et de recherche français ou étrangers, des laboratoires publics ou privés.

Linking eutrophication to carbon dioxide and methane emissions from exposed mangrove soils along an urban gradient

Glenda C. Barroso[1,2], Gwenaël Abril[1,3], Wilson Machado[1,2], Rodrigo C. Abuchacra[4], Roberta B. Peixoto[1,2], Marcelo Bernardes[1], Gabriela S. Marques[1], Christian J. Sanders[5], Gabriela B. Oliveira[2], Silvio R. de Oliveira Filho[6], Leonardo Amora[2,6], Humberto Marotta[1,2,6]

Science of the Total Environment 850, https://doi.org/10.1016/j.scitotenv.2022.157988.

[1]Graduate Program in Geosciences (Environmental Geochemistry), Fluminense Federal University (UFF). Outeiro São João Baptista, s/n, 24020-007, Niterói, Brazil.

[2]Ecosystems and Global Change Laboratory (LEMG-UFF)/Brazilian Ocean Acidification Network (BrOA), Biomass and Water Management Research Center (NAB-UFF), Fluminense Federal University (UFF), Av. Edmundo March, s/n°, Niterói, RJ, Brazil, 24210-310.

[3]Laboratoire de Biologie des Organismes et Ecosystèmes Aquatiques (BOREA), UMR 8067, Muséum National d'Histoire Naturelle, CNRS, IRD, SU, UCN, UA, 43 rue Cuvier, CP 26, 75231 Paris Cedex 05, France.

[4]Department of Geography, Graduate Program in Geography, State University of Rio de Janeiro (FFP), Rua Dr. Francisco Portela, 1470 São Gonçalo, 24435-005, Rio de Janeiro, Brazil

[5] National Marine Science Centre, Faculty of Science and Engineering, Southern Cross University, Coffs Harbour, NSW 2540, Australia

[6]Physical Geography Laboratory (LAGEF-UFF), Department of Geography, Graduate Program in Geography, Fluminense Federal University (UFF), Av. Gal. Milton Tavares

de Souza, s/n°, Niterói, RJ, Brazil, 24210-346

*corresponding author: humbertomarotta@id.uff.br

Graphical Abstract

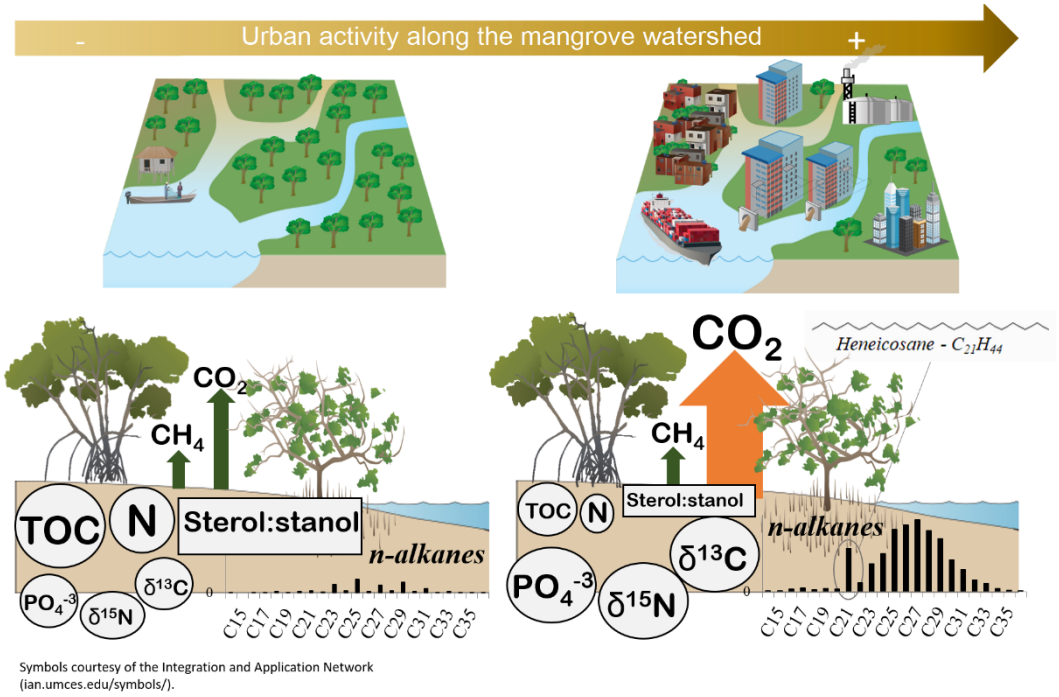

HIGHLIGHTS

- Elementary, isotopic, and molecular proxies indicated mangrove organic matter lability;
- Organic matter lability increased with urban growth and untreated sewage discharges;
- Carbon dioxide emissions from exposed mangrove soils increased with eutrophication;
- Methane emissions were 3 orders of magnitude lower than dioxide carbon emissons;
- n-alcanes and sterol biomarkers suggest enhanced biomass degradation with pollution.

Abstract

Mangroves are one of the most important but threatened blue carbon ecosystems globally. Rapid urban growth has resulted in nutrient inputs and subsequent coastal eutrophication, associated with an enrichment in organic matter (OM) from algal and sewage sources and substantial changes in greenhouse gas (GHG) emissions. However, the effects of nitrogen (N) and phosphorus (P) enrichment on mangrove soil OM composition and GHG emissions, such as methane (CH_4) and carbon dioxide (CO_2), are still poorly understood. Here, we aim to evaluate the relationships between CO_2 and CH_4 efflux with OM composition in exposed soils from three mangrove areas along watersheds with different urbanization levels (Rio de Janeiro State, Brazil). To assess spatial (lower vs. upper intertidal zones) and seasonal (summer vs. winter) variability, we measured soil-air CO_2 and CH_4 fluxes at low spring tide, analyzing elementary (C, N, and P), isotopic ($\delta^{13}C$ and $\delta^{15}N$), and the molecular (n-alkanes and sterols) composition of surface soil OM. A general trend of OM composition was found with increasing urban influence, with higher $\delta^{15}N$ (proxy of anthropogenic N enrichment), less negative $\delta^{13}C$, more short-chain n-alkanes, lower C:N ratio (proxies of algal biomass), and higher epicoprostanol content (proxies of sewage-derived OM). The CO_2 efflux from exposed soils increased greatly in median (25/75% interquartile range) from 4.6 (2.9/8.3) to 24.0 (21.5/32.7) mmol m^{-2} h^{-1} from more pristine to more urbanized watersheds, independent of intertidal zone and seasonality. The CO_2 fluxes at the most eutrophicated site were among the highest reported worldwide for mangrove soils. Conversely, CH_4 emissions were relatively low (three orders of magnitude lower than CO_2 fluxes), with high peaks in the lower intertidal zone during the rainy summer. Thus, our findings demonstrate the influence of coastal eutrophication on global warming potentials related to enhanced heterotrophic remineralization of blue carbon within mangrove soils.

Keywords: CO_2; CH_4; Nutrient; Urban Growth; Organic Matter.

1. Introduction

Recent scientific evidence indicates that increased organic matter (OM) and nutrient flows to coastal areas are critical components of global change, resulting in the degradation of biodiversity, water quality, and C storage (Breitburg et al., 2018).

Eutrophication can be defined as an increased rate of OM supply to an ecosystem, not as a trophic state but as a process (Nixon, 1995). Nutrient and OM inputs from natural sources may be increased due to cultural eutrophication associated with urban sewage loading and enhanced coastal productivity. Eutrophication has become widespread in coastal marine environments around the world (Jiao et al., 2018; Häder et al., 2020). Substantial changes in sources and quality of OM deposited in aquatic sediments have been widely reported following eutrophication (Alongi, 2009; Kristensen et al., 2017).

Soils are the main organic carbon (OC) pool in mangrove ecosystems (Hamilton and Friess, 2018). These pools are referred to as blue C, an important component of the marine C cycle. (Jiao et al., 2018). However, the large blue C stocks in these systems may be partially remineralized to greenhouse gases (GHGs) and returned to the atmosphere (Jacotot et al., 2018; Martin et al., 2020). Despite their importance to global climate and biodiversity, mangroves have been heavily threatened by deforestation (Hamilton and Friess, 2018) and cultural eutrophication (Barcellos et al., 2019). Previous studies have indicated contrasting effects of eutrophication on C storage in mangrove soils, such as enhanced OM accumulation (Sanders et al., 2014) and remineralization (Queiroz et al., 2020).

The principal GHG released from mangrove soils is CO_2, as this gas may be derived from a wide variety of aerobic and anaerobic diagenetic reactions (Alongi, 2009). In turn, CH_4 production is a strictly anaerobic process and limted in coastal wetlands due to high sulphate concentrations from seawater. High sulphate concentrations favor OM degradation through sulphate reduction rather than methanogenesis (Martens and Berner, 1974). However, eutrophication and subsequent enrichment of labile organic substrates may stimulate methanogenesis in these environments (Chen et al., 2011).

Although several studies have demonstrated changes in OM composition and C cycling processes in mangroves undergoing eutrophication (Sanders et al., 2014; Keuskamp et al., 2015; Pérez et al., 2020), a better understanding of the mechanistic links between GHG emissions and the quality of natural and anthropogenic OM is still needed. Highly variable CO_2 and CH_4 emissions from mangrove soils are also commonly attributed to the effects of biogenic structures (e.g., crab burrows and pneumatophores) that promote oxygenation and gas diffusion (Ouyang et al., 2016). As a result, differences in subaerial exposure time observed between the lower and upper intertidal zones are also a critical control of redox conditions to biogeochemical processes in mangrove soils (Kristensen et al., 2017). In addition to spatial variation from lower to upper intertidal zone, the physical, chemical, and biological drivers of GHG emissions may vary temporally over the seasonal cycles, especially due to variation in temperature and/or rainfall (Kristensen et al., 2008a; Jacotot et al., 2019).

Diverse spatial and seasonal responses of highly dynamic GHGs to eutrophication remain poorly understood for a wide intra- (Chen et al., 2012) and inter- (Kristensen et al., 2017) variation of mangrove soils. This study aims to assess the relationship between OM composition (elementary, isotopic, and molecular proxies), biological structures (crab burrow and pneumatophore densities), and GHG emissions (CO_2 and CH_4) from three mangrove soils, with different urbanization levels along specific watersheds within the Rio de Janeiro State, Southeastern Brazil. Our hypothesis was that higher CO_2 and CH_4 emissions would be associated with increasing cultural eutrophication indicated by OM elementary, isotopic, and molecular composition in mangrove soils, independent of intertidal zone and seasonality. To address these assumptions, soil-atmosphere C exchange rates were compared during low spring tides, taking into account differing spatial scales among mangroves and their intertidal zones (lower vs. upper intertidal zones), as well as seasonal variability (summer vs. winter).

2. Methods

2.1. Sampling area and possible eutrophication sources within catchments

This study was conducted in three mangroves along the inner parts of semi-enclosed bays within a relatively close distance of ~160 km along the shoreline of the Rio de Janeiro State (Southeast Brazil). Each study site is shown on Figure 1: Saco de Mamanguá (M1), Guapimirim (M2) and Guaratiba (M3). For each mangrove area, two sites were established considering differences in the topographic profile and dominant vegetation composition: the lower and upper intertidal zones situated at fringe and basin forests, respectively (Fig 1). This classification assumes that fringe forests have higher frequency of tidal inundation than basin forest in the innermost zone, as described by Schaeffer-Novelli et al. (2000). The lower zone here is dominated by *Avicennia schaueriana* in M1 and M3 and *Laguncularia racemosa* in M2*,* while in the upper zone of these mangroves *Rhizophora mangle* is most prevalent (Table S1).

The climate of the region according to Köppen-Geiger classification is tropical with wet summers and dry winters (Aw). The 12-year (2007-2019) monthly averages of temperature and accumulated rainfall in the three study regions vary from ~21 to ~26°C and ~121 to ~475mm in winter and summer, respectively (data provided by the Brazilian National Institute of Meteorology, stations A602 and A619 located ~4 and ~12 km from M3 and M1, respectively, and by the Brazilian Airspace Control Institute, station 83746 located ~24 km from M2). Monthly mean temperature and accumulated rainfall data in each sampling season and region were provided by meteorological stations A602 and A619 (available at https://portal.inmet.gov.br/) and 83746 (available at https://www.redemet.aer.mil.br/). The micro-tidal regime of M1, M2 and M3 mangroves

149 is predominantly semidiurnal, averaging 0.75, 0.76 and 0.43m, respectively, as estimated
150 using the software PACMARE (Franco, 1997).

151 M1 is a small and well-preserved ecosystem inside an elongated cove with
152 restricted water circulation, which receives oligotrophic waters from pristine inland and
153 marine environments, located within the Cairuçu Environmental Protection Area in the
154 west portion of the Ilha Grande Bay. Also, the watershed of the M1 mangrove is very
155 small, with a low local river freshwater discharge (Brandini et al., 2019). In contrast, M2
156 site is influenced by eutrophic and mesotrophic rivers, even considering that this site is
157 located within the Guapimirim Environmental Protection Area in Guanabara Bay
158 (Carreira et al., 2001). Lastly, the M3 site is located within Sepetiba Bay, also situated at
159 a conservation area (State Biological Reserve of Guaratiba), though highly impacted due
160 to continuous domestic and industrial sewage discharges from a highly urbanized
161 catchment area (Copeland et al., 2003; Marins et al., 2004). Although the entire drainage
162 basin of Guanabara Bay is one of most urbanized in Brazil (Amador, 2013), with an
163 estimated population ~17 million compared to ~1.8 million in of Sepetiba Bay (IBGE,
164 2010), the immediate watershed of the M2 site is much less urbanized than that of M3
165 (Table S1, Fig 1).

166 The urban growth along the Rio de Janeiro coastline occurred with a low level of
167 wastewater treatment (Fistarol et al., 2015), contributing to the eutrophication of
168 Guanabara and Sepetiba Bays, where M2 and M3 mangroves are respectively located
169 (Figure 1). In constrast, the Ilha Grande Bay, including the cove where M1 is situated,
170 remains relatively pristine (Abril et al., 2022). During the sampling period, the increased
171 eutrophication in surface waters around M3, eastern portion of Sepetiba Bay, is confirmed
172 by the highest DO saturation and inorganic nutrient concentrations (Table S2), which are
173 typically associated with eutrophication in coastal waters (Marotta et al., 2012). As an

174 evidence of eutrophication sources in the study area, data from the Rio de Janeiro State
175 Environmental Institute (N = ~4 monthly samples per 3-6 contributing river of each bay
176 portion from 2017 to 2018, available at http://www.inea.rj.gov.br) indicate biochemical
177 oxygen demand, total phosphorus (TP) concentrations, and fecal coliform counts above
178 1.5, 2.5, and 3.5 times higher, respectively, in tributaries near M2 than those of M1. The
179 highest eutrophication in tributaries near M3 is represented by these water parameters
180 above 6, 20, and 170 times higher, respectively, compared to those of M1.

181 2.2. Study Design

182 Samples were taken from each mangrove area: most pristine (M1), intermediate
183 (M2) and most urban (M3). Sampling included measurements of soil-air CO_2 and CH_4
184 fluxes associated with OM elementary, isotopic, and molecular compositions and
185 biogenic structures. Sampling sites included the lower (L) and upper (U) intertidal zones
186 and samples were taken in winter ("W"; July-September 2017) and summer ("S";
187 February-March 2018) at low spring tide.

188 Gas chambers (N=3-5 and 7 for CO_2 and CH_4, respectively) were randomly
189 distributed in the same day between 08:00 and 13:00 local time at both zones for each
190 mangrove. After gas sampling, the aboveground density of pneumatophores of *Avicennia*
191 *schaueriana* and crab burrows were counted. Then, surface soil samples (~2 cm) for OM
192 composition and granulometric analysis were taken from the area under each chamber where
193 CO_2 and CH_4 emissions were measured. For PCA and correlation analysis, each data of
194 biogenic structures, soil composition, and GHG flux was the median for each upper or lower
195 zone, mangrove ecosystem, as well as winter or summer (N = 12). At each upper or lower
196 intertidal zone of mangrove, samples of live leaves, stems, and roots of the dominant
197 species (*Rhizophora mangle*, *Avicennia shaueriana* or *Laguncularia racemosa*) were still
198 collected (N = 3 samples of plant material from each of 3 individuals per species) to

199 determine isotopic composition of these potential endmembers. Lastly, the topography of
200 each ecosystem was measured along transects from the lower and upper intertidal zones
201 to estimate the number of days in which soils are annually exposed or flooded by tides in
202 each sampling site.

203 2.3. Analytical Methods

204 2.3.1. Gas Emissions from the Exposed Soil-Air interface

205 a) Exposed soil-air CO_2 exchange rates

206 Short-term measurements of CO_2 concentration (ppm) were taken inside Plexiglass
207 chambers (volume of 5776 cm^3 and area of 268 cm^2; N = 3-5 chambers measured 3-7
208 times each one) coupled in a closed system with a previously calibrated infrared gas
209 analyzer (Licor, LI-820). To minimize disturbance of surface roots or other biogenic
210 structures, these chambers were gently inserted ~2 cm into the soil, permitting the
211 quantification of CO_2 exchange rates as a function of the linear increase gas concentration
212 inside the chambers (Rochette and Hutchinson, 2015). After closing the system and
213 reaching atmospheric levels (± 10%), the CO_2 concentrations were measured every
214 second during a short incubation period of ~8 min to avoid bias on gas diffusivity by
215 artificial changes, especially in temperature (Kabwe et al., 2002).

216 b) Exposed soil-air CH_4 exchange rates.

217 These fluxes were measured with the static closed chamber method, derived from
218 significant linear slopes ($p<0.05$) only with a $R^2> 0.80$ of gas concentration versus time
219 to ensure accurate measurements. We used 3-5 discrete air samples for CH_4
220 concentrations, of which were taken at ~30-45 min intervals over 90-160 min inside
221 chambers. For detection purposes, low rates require longer incubation times. Seven
222 Plexiglass chambers (volume of 5,776cm^3 and area of 268cm^2) were gently inserted ~2
223 cm into soils and placed randomly around a 10-20m distance in each studied zone, season,

and mangrove (Hutchinson and Livingston, 2001). To reach the atmospheric equilibrium before the initial time, chambers were opened for ~20-min through a gas valve (Keller et al., 2000). Air samples were carefully collected after being homogenized inside each chamber, using a 20-mL gas-tight syringe, and transferred to pre-evacuated 12-mL glass vials (Exetainer®, Labco, UK). Then, these vials were kept at room temperature, transported, and analyzed in the laboratory using a previously calibrated Agilent gas chromatograph (model 7890B) equipped with flame ionization detector and nickel catalytic methanizer.

c) Calculations of exposed soil-air gas exchange rates

CO_2 or CH_4 fluxes across the exposed soil-air interface (F) were calculated from the linear regression of each gas concentrations inside chambers versus time (only values of R^2>0.8 were used), following the Eq. (1):

$$F_{(CO2,\ CH4)} = (d\ (CO_2,\ CH_4)/\ dt).\ (P.V)/\ (R.T.S)$$

where F is the CO_2 or CH_4 flux from exposed soils to the atmosphere (CO_2: mmol m^{-1} h^{-1}; CH_4: µmol m^{-2} h^{-1}); d (CO_2, CH_4/dt) is the variation in CO_2 or CH_4 concentrations as a function of time (ppm s^{-1}), P is the atmospheric pressure (µatm), V is the total chamber volume (m^3); R is the ideal gas constant of 820528 x 10^{-05} (atm m^3 K^{-1} mol^{-1}), T is the absolute air temperature (K), and S is the surface area covered by the incubation chamber (m^2).

2.3.2. Chemical composition of Mangrove Soils and Endmembers

Analysis of elementary (C, N, P), isotopic ($\delta^{13}C$ and $\delta^{15}N$), and molecular (sterols and n-alkanes) composition of OM, and soil grain-size were performed in ~2 cm depth surface soils inside each of the CO_2 and CH_4 flux chambers, totalizing 84 samples (14 samples per mangrove zone and season). Fresh leaves, stems, and roots considered as endmembers representatives were carefully washed with deionized water before freeze-

drying. The soil samples and plant material were kept at -20°C before being freeze-dried, grounded to powder, and stored in plastic containers for further analysis. Plant debris were removed when present in the soil samples before freezing.

a) Carbon and Nitrogen content and Isotopic composition

Prior to OC and $\delta^{13}C$ analysis, soil samples were acidified (10% HCl) as described by Wendlandt (1986) to eliminate carbonates, while soil for TN, $\delta^{15}N$ analysis and all plant samples were not acidified. Both acidified and non-acidified dry-powder soil samples were weighted (10-20 and 6-8 mg sealed in silver and tin capsules for soils and plant tissues, respectively), and the analysis were carried out using a Flash Element Analyzer coupled to a Thermo Fisher isotope ratio (Delta V IRMS) mass spectrometer. Analytical precision was as follows: C=0.1%, N=0.1%, $\delta^{13}C$=0.1‰, and $\delta^{15}N$=0.15‰.

b) Phosphorus content

Total phosphorus (TP) was determined after calcination at 450°C for 4h, while inorganic phosphorus (IP) in freeze-dried samples. IP was determined in soil samples extracted with 1N-HCl after stirring for 16 hours, using the ascorbic acid/molybdenum blue colometric method at 880nm (Grasshoff et al., 1999). In turn, the organic phosphorus (PO) was calculated as the difference between total and inorganic P fractions. The absorbance was measured using a Shimadzu UV-1601PC spectrophotometer.

c) Lipid biomarkers

The n-alkane and sterol extractions were performed in dry-powder soil samples (~2g) following EPA (1996) as adapted by Wakeham and Canuel (1988). The extraction was carried out using ultrasonic baths of dichloromethane (DCM), DCM: methanol (1:1), and methanol (2x). After centrifuge the supernatants, complete reduction in roto-evaporate and transfer to a chromatographic column, the n-alkanes were obtained eluting 3 ml of n-hexane, while sterols were eluted with 3.5 ml of hexane and ethyl acetate (3:1).

Analysis was performed in a GC-FID 7890A HP-Agilent fitted with a DB-5 capillary column (30m, 0.32mm, 0.25µm). Derivatization was performed prior to sterols analysis. The n-alkanes and sterols were identified in comparison with commercial standards, Surrogates (C30D64 and androstanol) and internal standards (C24D50 and 5a-cholestane), respectively. Detection limit for alkanes was 0.005 ng g^{-1} and for sterols 0.01 ng g^{-1}. Due to highly variable OC (Table 2), sterol concentrations were normalized to the organic carbon content (µg $gOrgC^{-1}$).

To distinguish natural matter sources from anthropogenic impacts, the following proxies were used. For sterols: (I) phytosterols (campesterol, stigmasterol and β-sitosterol) were applied for higher plant or phytoplankton, (II) the sum of coprostanol and epicoprostanol for sewage, and (III) cholesterol and cholestanol for plankton (Mannino and Harvey, 1999). In addition, coprostanol is abundant in untreated domestic sewage, while epicoprostanol is typically low in that untreated (Mudge and Lintern, 1999) and increased by the cholesterol reduction during the sewage treatment, being a proxy of treated sewage (McCalley et al., 1981).

Then, the 5β:(5β+5α) ratio (coprostanol:(coprostanol+colestanol) was used as a proxy of fecal contamination (Grimalt et al., 1990), while the coprostanol:cholesterol ratio (Cop:Cho; Mudge and Bebianno, 1997) pointed for sewage influence versus microbial degradation process and the diagenetic ratio stanol:stenol (Nishimura and Koyama, 1976; McCaffrey, 1990) indicated the proportion between fresher phytosterols and their degraded forms (campestanol, stigmastanol and β-sitostanol). For n-alkanes we used the indexes: (1) Terrestrial:Aquatic Ratio (TAR; Bourbonniere and Meyers, 1996) assumed here as (C27+C29+C31):(C15+C17+C19) ratio, in which values > 1.0 indicate the predominance of compounds from terrestrial or mangrove higher plants rather than algae; (2) the input of total n-alkanes (∑C14-40); (3) Carbon Preference Index (CPI; Clark

299 Jr. and Blumer, 1967) represented here as $\sum(C_{odd}(15\text{-}39):\sum(C_{even}(14\text{-}40)$, in which CPI <
300 1 indicates anthropogenic inputs, while CPI > 1.0 indicates biogenic sources; (4) Low
301 Molecular Weight:High Molecular Weight Ratio (LMW:HMW, Wang et al., 2006)
302 represented here as $\sum$(C14-23:$\sum$(C24-40) which was used to attribute aquatic over
303 terrestrial input; and (5) Pristane:Phytane ratio (Pr:Ph, Steinhauer and Boehm 1992) was
304 used as a proxy for redox conditions.

305 2.3.3. Grain Size

306 This procedure was carried out in dry soil samples free of carbonates and organic
307 compounds. Carbonates were removed by adding 20mL of HCl 1M for 48 hours followed
308 by washing and centrifugation with deionized water (5min at 3500rpm), while OM was
309 removed by loss on ignition at 400°C overnight (Schumacher, 2002). In addition, the
310 samples were disaggregated with 20mL of 4% sodium hexametaphosphate dispersant and
311 stirred on an orbital shaker for 24 hours, and subsequently sieved with a mesh diameter
312 of 420μm before laser diffraction analysis using a CILAS 1064 (0.04-500μm range). The
313 grain-size distribution was classified according to the Wentworth scale adopted in the
314 GRADISTAT routine, assuming the statistical parameters of Folk and Ward (1957).

315 2.3.4. Topography and Annual Period of Soil Exposure in Mangroves

316 Topographic profiles of mangrove soils from the lower to the upper intertidal zone
317 were measured with a Leica TS06 Total Station at low spring tide (e.g., Moser et al.,
318 2007; Wheaton et al., 2009). The vertical and horizontal distances of a transversal profile
319 were converted into altimetry using the sea level at the lower intertidal zone (*i.e.*, initial
320 seaward edge) with a GPS receiver (planimetric accuracy of ±3m). Then, the transect was
321 adjusted using the azimuth angle (magnetic north) at specific measured coordinates (Lam
322 and Chen, 2001), considering the mean sea-level which was established by the Brazilian
323 Navy as the altimetric reference. At the mangroves M1 and M3 sites, topographic profiles

were measured from the lower to the upper intertidal zones. In turn, two topographic profiles were surveyed at the M2 site due to logistical constraints, associated with highly unstable muddy substrate along single transects.

Additionally, between January 2017 and December 2018, we modeled 10-min interval tidal heights based on the harmonic method using the PACMARE software (Franco, 1997), which allows to calculate the annual mangrove soil subaerial exposure and flooding in each zone by the difference between the predicted tide height and the measured topography (Verhoeven et al., 2014). The tide gauge data derived from tidal height measurements and harmonic parameters were established by the Brazilian Navy (*https://www.marinha.mil.br/chm/tabuas-de-mare*).

2.4. Statistical analysis

The data in this study did not show significant homoscedasticity (Bartlett, $p>0.05$) and normal distribution (Kolmogorov-Smirnov, $p<0.05$) even after different transformations (Zar, 1996). For this, the Mann-Whitney test (significance level $p<0.05$) was used to compare two categories (e.g., upper and lower intertidal zones or summer and winter), while the Kruskal-Wallis test (significance level $p<0.05$) three or more (e.g., M1, M2, and M3 or intertidal zones in each mangrove and/or season). As post-test, differences were assessed with False Discovery Rate (FDR; significance level $p<0.05$), considering p-values from Mann-Whitney tests and the two-stage step-up method described by Benjamini et al. (2006). FDR is also more appropriate for environmental data that involved many multiple comparisons and small samples (García, 2004).

In addition, spearman correlation matrix (significance level $p<0.05$) and principal component analysis (PCA) were applied to find out the major controls on CO_2 and CH_4 emissions from mangrove soils (N = 12 including 2 intertidal zones, 2 seasons and 3 mangroves for each variable). The PCA was used to assess the magnitude and direction of

correlations between both dependent (soil-air CO_2 and CH_4 fluxes) and other independent variables. All statistical tests were performed using GraphPad Prism (version 7.0), except the PCA in Statistica software (version 10).

3. Results

The three studied mangroves showed significant heterogeneity in soil OM composition and urban growth along watersheds (Table 1), indicating a higher spatial (among mangroves and intertidal zones) than seasonal (summer *vs.* winter) variability as detailed below.

3.1. Elementary and Isotopic Composition of Soils

The surface soil of the studied mangroves was predominantly composed of silt (71-93%) and clay (4-17%; Table 1). Comparing the three systems, M1 showed ~2 times higher OC concentration than M2 and M3 (FDR, $p<0.05$; Fig 2). TN, OP, OC:TN and OC:TP ratio were ~2-4 times higher in M1 than in M2 and M3 (FDR, $p<0.05$; Fig 2; Table 1). $\delta^{15}N$ was ~ 5 times higher in M3 than in M1and $\delta^{13}C$ was ~20% higher in M3 than in M1 and M2 (FDR, $p<0.05$; Fig 2). In addition to being the highest in median, the $\delta^{13}C$ data showed the highest variation in M3 (25/75% interquartile) when compared to M1 and M2 (from -28 to -11‰, from -31 to -24‰, and from -32 to -26‰, respectively; FDR, $p<0.05$; Fig 2; Table 1). Median IP concentration was similar between M2 and M3, being ~70% higher than M1 (FDR, $p<0.05$; Fig 2). M2 showed the highest median (25/75% inter-quartil) values of TP concentration, since M1 = 1010 (908/1180), M2= 1202 (1054/1338), and M3= 1072 (1001/1150) $\mu g\ g^{-1}$ (FDR $p<0.05$; Fig 2). Only in M1 site, the OP was the predominant P form (Fig 2).

In relation to intertidal spatial variability of element composition, OC, TN, TP, δ13C, δ15N, C:N, C:P, and OP were from ~10 to 40% higher in the upper than in the lower zone, except IP that decreased ~10% (Mann-Whitney, significance level $p<0.05$; Fig S1). The seasonal variability between winter and summer was not significantly different for values of OC, TN, TP, $\delta^{15}N$, C:N, and C:P ratio (Mann-Whitney, $p>0.05$; Fig S2). However, $\delta^{13}C$ and IP were significantly higher and OP lower in winter compared to summer (Mann-Whitney, $p<0.05$; Fig S2). Moreover, the highest soil OC concentrations were found in the upper intertidal zone of M1 in both summer and winter seasons, contrasting with the lowest values in the lower zone of M3 in winter (FDR, $p<0.05$; Fig S3).

In the studied soils, 10 sterol compounds were identified (Table S3 and Table S4), and the total concentrations ranged from not detectable to 57.4 μg g^{-1}. β-sitosterol and stigmasterol showed a greater participation in the sterol pool in M1, and coprostanol (5β-cholestan-3β-ol) in M3. Highest concentrations of epicoprostanol (5β-cholestan-3α-ol) were found in M3, and often below the detection limit in M1 and M2. In contrast, the intermediate compounds of the diagenetic degradation of sterols, *i.e.* cholesterol (cholest-5-in-3β-ol) and cholestanol (5α-cholestan-3β-ol), varied among mangrove sites. These results indicate the highest cholesterol values in M2, variability of cholestanol in M3, and diagenetic ratio (stanol:sterol) in M3 (Table S3). Finally, a greater contribution of higher plants and algae sources in M1 and M2 (~60% to 79% of campesterol, stigmasterol, and β-sitosterol) contrasted with the highest influence of sewage in M3 (~3% to 11% of coprostanol and epicoprostanol; Fig. 4).

The total n-alkanes ($\sum Cn_{14-40}$) ranged from 186.3 in M1 to 4,021.1 μg $gOrgC^{-1}$ in M2, with an overall predominance of odd long chains (Cn_{25-29}). The dominant compounds were Cn_{25} in M1, while Cn_{25}, Cn_{29} and Cn_{31} in M2 and M3 being Cn_{21} more abundant in M3 (Table S5). In turn, all studied zones showed LMW:HMW ratio lower than 1, with

maximun and minimun values of CPI in M1 and M3, respectively. The TAR values in the upper zone of M3 were from 2 to 10 times lower than in other mangroves. Although maximum values of pristane and phytane were ~3 and 5 times higher in M3, the Pr:Ph ratio was less variable and ranged from 0.2 to 0.6 among mangroves (Table S3).

3.2. Isotopic composition of mangrove plant tissues

No significant difference in median of $\delta^{13}C$ values from leaves; stems and roots were observed among M1, M2, and M3 in upper and lower zones (Kruskal-Wallis, $p>0.05$; Table 2; Fig. S4). However, $\delta^{15}N$ from mangroves tree stem and roots were up to 72% higher in the lower intertidal zone of the most impacted mangrove (M3) than in all sites of the most pristine ecosystem (M1) (FDR, $p<0.05$; Figs. 3 and S4). Similarly, $\delta^{15}N$ from mangroves tree leaves was up to 70% higher in the upper zone of M3 than in all sites of M1 (FDR, $p<0.05$; Figs. 3 and S4).

3.3. GHG efflux from exposed soils to the atmosphere

Soil-air CO_2 efflux varied from 0.7 to 86.7 mmol m^{-2} h^{-1} (Table 1), with higher values in the mangrove with the greatest urban growth along the watershed (M3), which were from near 60 and 30% higher on average than M1 and M2, respectively (FDR, $p<0.05$; Fig 5). Moreover, no significant spatial diferences within intertidal zones (upper vs lower) and seasonal difference (summer vs winter) in CO_2 fluxes were observed (Mann-Whitney, $p>0.05$; Fig 5).

CH_4 emissions were relatively low but showed a single peak of 1.69 of mmol m^{-2} h^{-1} in the lower intertidal zone of M2 in summer (Table 1). Despite no significant difference among the mangroves M1, M2, and M3 (Kruskall-Wallis, $p>0.05$), soil-air

CH4 fluxes were ~70% greater in lower compared to upper intertidal zones and summer to winter seasons (FDR, $p<0.05$; Fig. 5).

3.4. Topography, annual subaerial exposure time, and biological structures along mangrove soils

All topographic profiles here indicated a very subtle morphological change, with the soil elevation varying from 0.81 to 1.19, 1.12 to 1.18, and 0.88 to 1.32 m in relation to the Mean Sea Leval (MSL) between the lower and upper zones of M1, M2 and M3, respectively (Fig. S6). Our estimates calculated from topographic profiles and tide gauge data indicate that soils are exposed during 201 versus 333, 304 versus 320, and 303 versus 360 days annually at the lower and upper mangrove zones in M1, M2 and M3, respectively. As a result, the annual subaerial exposure time was ~66, 5, and 19% higher in the upper than lower zones of M1, M2 and M3, respectively. Regarding biological structures, crab burrow density showed an increasing trend from M1 and M2 to M3 soils, in median, 0 and 40 to 150 m^{-2}, respectively, while pneumatopheres did not follow any pattern, reaching 370, 70, and 240 m^{-2}, respectively.

3.5. Relationships between soil variables

Overall, OC was positively related to TN and OP, and negatively related to $\delta^{15}N$, $\delta^{13}C$ and IP ($rs = 0.90, 0.94, -0.87, -0.59$ and -0.88, respectively, $p<0.05$; Table S6 and Fig. 3). TN was positively related to OP, and negatively related to $\delta^{15}N$, $\delta^{13}C$, IP and crab burrow ($rs = 0.93, -0.95, -0.60, -0.87$ and -0.69, respectively, $p<0.05$; Table S6 and Fig. 3). $\delta^{15}N$ was positively related to IP and crab burrow, and negatively related to OP ($rs = 0.94, 0.73$, and -0.94, respectively, $p<0.05$; Table S6 and Fig. 3). $\delta^{13}C$ was positively related to crab burrow, and negatively related to OP ($rs = 0.82$ and -0.62, respectively,

447 $p<0.05$; Table S6 and Fig. 3). IP was positively related to crb burrow, and negatively
448 related to OP, while OP was negatively related to crab burrow (rs = 0.65, -0,91 and -0.70,
449 respectively, $p<0.05$; Table S6 and Fig. 3).

450 In turn, soil-air CO_2 fluxes were positively correlated to Σn-alkanes, $\delta^{15}N$, $\delta^{13}C$, IP
451 and crab burrow (rs = 0.74, 0,61, 0.70 and -0.65, respectively, $p<0.05$; Table S6 and Fig.
452 3), while CH_4 fluxes was positively related to Σn-alkanes and sandy (rs = 0.60 and 0.88,
453 respectively, $p<0.05$; Table S6 and Fig. 3). The sewage (coprostanol+epicoprostanol) was
454 positively correlated with 5β:(5β+5α) ratio (coprostanol:(coprostanol+cholestanol), $\delta^{15}N$,
455 and IP as well as negatively with TN (rs = 0.82, 0.64, 0.60 and -0.64, respectively, $p<0.05$;
456 Table S6 and Fig. 3). Finally, diagenetic ratio was positively correlated to crab burrow
457 (rs = 0.74, $p<0.05$; Table S6 and Fig. 3).

458 Considering data from all mangrove soils, CO_2 emissions were positively correlated
459 with the aboveground density of crab burrows (r_s = 0.65; $p<0.05$, Table S7), but no
460 significant relationships were observed with that of pneumatophore ($p>0.05$). Moreover,
461 CH_4 emissions were not significantly related with aboveground density of
462 pneumatophores and crab burrow.

463 The PCA showed that Factor 1 and Factor 2 together explained ~68 % of the total
464 data variance. Factor 1 (CO_2 fluxes) explained ~51 % of the total variance with positive
465 loadings for $\delta^{15}N$, IP, crab burrows, $\delta^{13}C$, sewage, Σn-alkanes, diagenetic ratio,
466 5β:(5β+5α), pneumatophores, OP and CH_4 fluxes versus negative loadings for TN, sandy
467 and OC. Factor 2 (CH_4 fluxes) explained ~17 % of total variance with negative loading
468 for diagenetic ratio, $\delta^{13}C$, crab burrows, sewage, 5β:(5β+5α), OC, TN, $\delta^{15}N$ and CO_2
469 fluxes versus positive loadings for Σn-alkanes, pneumatophores, OP, IP, sandy, and CH_4
470 fluxes (Fig 6, Table S8). Accordingly, the M1 mangrove was grouped at a negative
471 direction of Factor 1 similarly to OP, OC, and TN. The M3 mangrove was grouped at a

472 right direction of Factor 1 and positive direction of Factor 2 such as sewage (coprostanol
473 and epicoprostanol), 5β:(5β+5α) ratio (colestanol and coprostanol), diagenetic ratio
474 (stanol:sterol), IP, $\delta^{15}N$, and $\delta^{13}C$. The M2 mangrove displayed an intermediate position
475 with an exception in the lower zone in summer, which difference was likely driven by
476 CH_4 emissions and the percentage of sand in surface soils (Fig. 6; Table S8).

477 **4. Discussion**

478 4.1. Anthropogenic variations in sources, composition, and diagenesis of OM in
479 mangrove soils

480 The trend of eutrophication with urban growth along the watersheds here was
481 apparent by substantial differences in mangrove soil IP and OM. Mainly caused by
482 nutrient inputs and defined as an increase in the rate of supply of OM to an ecosystem
483 (Nixon, 1995), eutrophication has widely been indicated by proxies related to increased
484 algal biomass in benthic coastal marine environments (Dell'Anno et al., 2002; Lemley et
485 al., 2015). As found from M1 to M2 and M3, increased IP content (Wolters et al., 2016;
486 Barcellos et al., 2019), $\delta^{15}N$ and $\delta^{13}C$ values (Sanders et al., 2014), and OM lability
487 biomarkers (Kumar et al., 2019) have been largely attributed to increased algal and
488 sewage inputs associated with more intense diagenesis of OM.

489 Previous evidence based on pelagic chlorophyll-*a* satellite data confirms the
490 presence of dense algal blooms as a proxy of water eutrophication in Sepetiba Bay (site
491 M3) and Guanabara Bay (site M2), but not in Ilha Grande Bay where the M1 mangrove
492 is located (Abril et al., 2022). Hence, the present study gives a more detailed assessment
493 of the contribution of natural (*i.e.*, mangrove trees vs algae) and anthropogenic (*i.e.*,
494 sewage) sources of OM, as well as identifying recent diagenesis processes through the
495 proportion of fresh compounds and their degraded forms (stanol/stenol) in mangrove soils
496 with urban growth along their watersheds.

497 The bulk composition of soil OM was consistent with an additional dual source of
498 anthropogenic OM that mixes with material from mangrove trees in the study sites
499 impacted by urban discharges. The increasing $\delta^{15}N$ trend between mangrove soils (M1 <
500 M2 < M3) was consistent with what was found in the plant material, specifically
501 significantly higher values in tree leaves from M3 compared to M1. The $\delta^{15}N$ proxy has
502 shown to be a robust indicator of eutrophication as it traces N cycling from untreated
503 sewage to mangrove areas (Gritcan et al., 2016). The range of these soil variables in M3
504 have often been associated with the influence of algal blooms in coastal aquatic sediments
505 under nutrient-enriched conditions (Zhang et al., 2015), and was also observed in urban
506 mangroves receiving untreated wastewaters (Machiwa, 2000). Accordingly, only M3
507 soils presented both $\delta^{15}N$ and $\delta^{13}C$ values within the previously observed range of sewage
508 (Barros et al., 2010). In contrast, more negative $\delta^{13}C$ and higher C:N ratio in soils of the
509 upper intertidal zone of the most pristine mangrove (M1) suggests greater dominance of
510 OM from woody plants (Meyers, 1994; Lamb et al., 2006). This confirms the potential
511 role of tree biomass to fuel the net heterotrophy that was previously reported in its
512 surrounding bay waters (Brandini et al., 2019).

513 In addition, molecular analysis supported potential differences in soil OM quality
514 and source with increasing the urban activity along the watershed. As many sterols may
515 be from natural biomass, the total sterol concentrations in the most pristine mangrove
516 (M1) were much higher than previously reported in estuarine sediments undergone
517 sewage contamination (dos Reis Souza et al., 2020). For instance, the contributions of
518 stigmasterol and β–sitosterol were predominant in pristine M1 soil, consistent with
519 natural source from higher plants (mangrove trees leaves and roots; Nes, 1974). In turn,
520 the coprostanol concentration below 0.5 $\mu g\ g^{-1}$ in sediments of all sampling sites did not
521 indicate sewage contamination (González-Oreja and Saiz-Salinas, 1998; Carreira et al.,

2009). Even the mangrove soils with greater urban pressure along the watershed (M3) showed coprostanol concentrations similar to estuarine sediments not impacted (Muniz et al., 2006) or moderately impacted (Carreira et al., 2009) by sewage, as well as lower than those impacted (dos Reis Souza et al., 2020).

Conversely, sterol biomarker distributions indicate a higher contamination of mangrove soils with sewage OM in M3 than M2, compared to non-detectable levels in the most pristine M1. The highest epicoprostanol concentrations found in the M3 soils are typical of sewage contamination, as reported in many coastal bottom sediments in South America (Mudge and Seguel, 1999), Australia (Pratt et al., 2008), and Asia (Isobe et al., 2002; Jeng, 2006). The predominance of epicoprostanol in relation to coprostanol in M2 and M3 soils, independent of sampling site or season, also indicates intense biological degradation likely fueled by OM derived from sewage (Santos et al., 2008). Accordingly, higher values of the sum of epicoprostanol and coprostanol in M3, as a proxy of sewage (McCalley et al., 1981), explains the positive relationships in the correlation matrix and PCA analysis to other indicators of eutrophication in mangrove soils here, including 5β:(5β + 5α), IP, and $\delta^{15}N$. The sewage contamination in M3 was further indicated by the coprostanol:cholesterol ratios (chop:cho) higher than 1.0 (Mudge and Bebianno, 1997) and coprostanol:cholestanol 5β:(5β + 5α) higher than 0.5 (Santos et al., 2008), as reported in tropical coastal aquatic sediments receiving high sewage discharges (Frena et al., 2016; dos Reis Souza et al., 2020). This limit of 5β:(5β + 5α) ratio of 0.5 for sewage pollution is assumed lower at tropical than non-tropical latitudes due to higher microbial activity with increasing temperature (Araujo et al., 2011).

Concerning n-alkanes, the CPI index higher than 1.0 in all studied mangrove soils, confirmed a large contribution of biogenic sources rather than petrogenic sources (Kumar et al., 2019). In particular, LMW:HMW ratio lower than 1.0 and TAR values above 1 at

547 all sampling sites confirm a dominance of high molecular OM weight from mangrove
548 trees (Gearing et al., 1976; Wang et al., 2006), as previously reported in mangroves
549 globally (Alongi et al., 1999; Kristensen et al., 2008a). Another proxy of OM sources
550 here was the overall predominance of long and odd chain of n-alkanes (Cn_{25-31}), still
551 indicating a large contribution from mangrove tree leaves (Eglinton et al., 1962;
552 Nishigima et al., 2001). In addition, exposed soil conditions might have favored oxidative
553 decarboxylation of fatty acids, also contributing to the predominance of odd-numbered
554 hydrocarbon chain (Guoying et al., 1980), except for the lower zone M2 during summer
555 and the lower intertidal zone of M3 during winter, likely due to petrogenic sources and
556 biological remineralization of OM (Thomazelli, 2010). Petrogenic sources of OM are
557 reasonable in M2 and M3 due to the high influence of industrial plants and ship traffic in
558 Guanabara Bay (Fistarol et al., 2015) and Sepetiba Bay (Molisani et al., 2006),
559 respectively.

560 The CPI index still above but closer to 1.0 in M3 soils typically indicate greater
561 abundance of low molecular weight n-alkanes than M1 and M2, which may be derived
562 from phytoplankton, bacteria, fungi and/or contamination by petroleum products (Boehm
563 and Requejo, 1986; Wang et al., 2003). In these mangrove soils of which was most
564 influenced by urban watershed, a greater abundance of short-chain n-alkanes Cn_{15-21}
565 indicates an additional contribution of phytoplankton and bacteria (Clark Jr. and Blumer,
566 1967; Canuel et al., 1997), a common effect of intense metabolic processes under coastal
567 eutrophication (Breitburg et al., 2018). Indeed, the lowest values of TAR observed in the
568 upper zone of M3 confirmed a lower relative contribution of vascular plants in the
569 mangrove to the n-alkane pool in the soil at this impacted site (Carreira et al., 2009). The
570 highly reducing anaerobic conditions of organic mangrove soils were still supported by
571 the values of Pr:Ph ratio below 1.0 in all sampling sites. Both n-alkane and sterols
572 biomarkers thus converge to the idea of a net gradient of increasing contributions not only

573 of sewage derived OM but also algal (phytoplankton and/or microphytobenthos) derived
574 OM from M1 to M2 and M3.

575 Besides differences in OM sources, the organic C and P contents were significantly
576 higher in the most pristine mangrove M1 (particularly along the upper intertidal zone)
577 than in the more impacted mangroves M2 and M3. This trend contributes to the negative
578 relationships between OC with IP, $\delta^{15}N$ and $\delta^{13}C$ found in the correlation matrix and PCA
579 analysis. A likely explanation is that local rivers around M2 (Faria and Sanchez, 2001)
580 and M3 (Borges and Nittrouer, 2016) promote a higher discharge of suspended matter
581 (i.e., OM dilution by inorganic sediment loads). This greater discharge of suspended
582 matter is related to deforestation and river straightening along the urban watersheds of
583 M2 and M3. In contrast, the more pristine mangrove (M1) is associated with a lower river
584 flow and more enclosed geomorphology of which could have contributed to the higher
585 OC content at this mangrove.

586 Furthermore, previous experimental evidence has indicated that total C and N
587 stocks may decrease from more pristine to more impacted mangrove soils, as an effect of
588 increased OM remineralization under anthropogenic-derived nutrient enrichment from
589 untreated effluents (Palacios et al., 2021). The higher diagenetic ratio in the most
590 eutrophicated M3 soils is a typical proxy of intense biological degradation of OM (Frena
591 et al., 2016), especially when stanol forms are dominant (i.e., this diagenetic ratio > 1.0;
592 Nishimura and Koyama, 1977). In contrast, M1 and M2 soils showed lower than 0.5
593 diagenetic ratios. The phytosterol:OC, C:N and C:P ratios were also higher in M1 and M2
594 soils compared to M3, particularly in the upper intertidal zone soil of M1, indicating that
595 OM is more preserved at these sites.

596 Considering the variability between lower and upper intertidal zones, a higher
597 influence of marine OM was still observed in mangrove soils of the lower than upper

598 zone, a potentially important effect of the increased inputs of marine compounds from
599 higher tidal inundation frequency near the sea (Sanders et al., 2010b). Trees retain woody
600 biomass within their roots, also increasing the nutrient uptake and light attenuation, which
601 could explain the reduced algal composition in soils of the upper intertidal zone (Sanders
602 et al., 2010a, 2014). In addition, more subaerial oxygenation throughout the year could
603 enhance phosphate adsorption by iron oxyhydroxides (FeOOH-PO_4; (Sherman et al.,
604 1998) or the uptake from more dense mangrove vegetation (Servais et al., 2019)could
605 have contributed to decrease IP content in the upper as compared to the lower intertidal
606 zones of the studied mangroves.

607 4.2 Response of GHG fluxes to anthropogenic perturbations and other parameters

608 Overall, our nutrient (N and P), isotopic ($\delta^{13}C$ and $\delta^{15}N$), and molecular (sterols and
609 n-alkanes) analysis in the three studied sites allowed us to assess potential controls of OM
610 composition on soil-air CO_2 and CH_4 fluxes. We observed a substantial increase in CO_2
611 emissions among mangrove soils from more pristine to more urban areas, contrasting with
612 similarly low CH_4 fluxes, except a single except peak in the site with more river influence
613 (lower zone of M2). This partially confirm previous evidence on enhanced production of
614 GHGs due to increased biological remineralization of OM with organic pollution in
615 mangrove soils (Sotomayor et al., 1994; Yang et al., 2018). Moreover, the observed
616 positive relationship in the correlation matrix between the abundance of n-alkanes and
617 soil-air CO_2 and CH_4 fluxes suggests the role of organic substrates to enhance biological
618 activity that releases these gases (Guoying et al., 1980).

619 Substantially higher CO_2 emissions from exposed soils, mainly in the most
620 eutrophicated soil (M3), is comparable to highly sewage-impacted mangroves around the
621 world (*e.g.*, Chen et al., 2010; Jacotot et al., 2018). This indicates a potential mechanistic
622 link between the intense urban sprawl (*i.e.*, associated with untreated wastewaters) and

623 increased soil OM remineralization, which have been reported in mangrove soils
624 undergone eutrophication from urban sources (Chen et al., 2010; Martin et al., 2020).
625 Higher soil-air CO_2 fluxes with urban growth along the watersheds here confirm the
626 increased remineralization fueled by higher availability of labile OM from sewage and
627 algae, typically associated with eutrophication (Breitburg et al., 2018). As a result, the
628 highest proportion of fecal sterols and degraded phytosterols associated with less OC
629 content in M3 also corroborates the role of the more labile OM derived from
630 phytoplankton and sewage to produce CO_2 (Drake et al., 2020). Besides the amount of
631 organic substrates to biological remineralization, another explanation for the increased
632 CO_2 release in ecosystems is the priming effect, in which the inputs of labile OM with
633 high energy and nutrients contents lead to additional metabolic breakdown of the more
634 recalcitrant OM pool, contributing to enhanced emissions of this gas (Guenet et al., 2010).
635 Previous studies have reported that heterotrophic responses to more labile OM inputs are
636 potentualy a threat to coastal eutrophication and blue carbon preservation (Alongi et al.,
637 1999; Kristensen et al., 2008a). Indeed, experimental research over past decade has
638 indicated increased OM remineralization with CO_2 production by priming effect in a wide
639 variety of coastal marine sediments, such as from estuaries (Gontikaki et al., 2015),
640 seagrass meadows (Liu et al., 2020), as well as other subtidal and intertidal areas (Van
641 Nugteren et al., 2009).

642 In turn, the CH_4 emissions here was within the range often found in pristine to
643 impacted mangroves around the world (Kreuzwieser et al., 2003; Kristensen et al., 2008b;
644 Konnerup et al., 2014). The median CH_4 efflux ~70% is significantly higher and was
645 associated to an increase in temperature of ~6°C and rainfall of ~900% in summer in
646 relation to winter over 30 days before sampling (average between meteorological stations
647 near M1, M2, and M3, as described in the Methods section). This result could be
648 explained by enhanced methanogenesis under warmer conditions (Vizza et al., 2017;

649 Jacotot et al., 2019) and higher freshwater inputs (Rosentreter et al., 2018). Accordingly,
650 the lower intertidal zone closest to the river mouth into the sea (i.e., more susceptible to
651 episodic reductions in salinity) might have contributed to the single peak of CH_4
652 outgassing in the M2 lower intertidal zone in summer, suggesting that transient increases
653 in methanogenesis could be influenced by nutrient enrichment.

654 In general, CH_4 emissions from exposed soils to the atmosphere were three orders of
655 magnitude lower than those of CO_2, confirming earlier findings in mangroves in Southern
656 China (Chen et al., 2010, 2011) and Brazil (Nóbrega et al., 2016). This result is a potential
657 consequence of previous estimates indicating that methanogenesis rates represent only 1-
658 10% of the total carbon mineralization in mangrove soils (Alongi, 2009). Although the
659 positive relationship between eutrophication and CH_4 emissions is commonly reported in
660 coastal aquatic ecosystems (Purvaja and Ramesh, 2001; Konnerup et al., 2014), we found
661 no significant changes along the urban gradient. Methanogenesis is often high in
662 freshwater sediments, while in marine environments the competition with more energetic
663 redox reactions by oxygen (*i.e.*, aerobic respiration) and other electron acceptors present
664 in seawaters (*i.e.*, mainly sulphate; King, 1984) or even the CH_4 oxidation under high
665 oxygenation of exposed soils (Das et al., 2018) is high in coastal wetlands. Oxidation
666 (Kristensen et al., 2008a) and more efficient OM remineralization pathways (Nóbrega et
667 al., 2016) could be especially intense in exposed mangrove soils and explain non-
668 significant changes of CH_4 emissions with eutrophication as found here.

669 Regarding the biogenic structures, pneumatophere and crab burrow densities have
670 presented differing relationships with GHG emissions from the exposed mangrove soils
671 studied. The weak explanation in the PCA and non-significant correlation between
672 pneumatophore density and CO_2 efflux contrasts with previous studies, which have
673 indicated a significant role in the release this gas directly to the atmosphere (Kristensen

674 and Alongi, 2006; Kristensen et al., 2008a; Ouyang et al., 2016). On the other hand, the
675 positive relationship between crab burrow density and CO_2 emissions found in PCA and
676 correlation analyses has been confirmed in a wide variety of mangrove soils (Ouyang et
677 al., 2016; Tomotsune et al., 2020). This result has been attributed to increased aerobic
678 CO_2 production from microbial processes within mangrove soils under more oxygenated
679 conditions driven by crab bioturbation (Kristensen and Alongi, 2006). Here, the
680 increasing trend of crab burrow density in M3 soils contributed to the significant positive
681 relationships of these faunal structures not only with CO_2 emissions, but also with
682 parameters affected by eutrophication (*i.e.*, IP, $\delta^{15}N$, $\delta^{13}C$, and diagenetic ratio). Instead,
683 pneumatophere density did not increase in the most impacted mangrove, and as a result
684 significant relationships were not found. In turn, lower CH_4 emissions as compared to
685 CO_2 might have contributed to the weak explanation in the PCA analysis and non-
686 significant correlation with both biogenic structures.

687 In addition to the influence of anthropogenic and natural inputs of OM, the subaerial
688 exposure time is a critical component to determine GHG emissions in mangrove soils
689 during the ebbing period, due to expected variations in metabolic rates with flooding
690 (Alongi et al., 2020). As performed here, previous studies have reported hourly or daily
691 C gas fluxes exclusively under exposed conditions (*e.g.*, Kabwe et al., 2002; Kristensen
692 et al., 2008b; Chen et al., 2010; Nóbrega et al., 2016). On an annual basis, estimates of
693 GHG emissions have assumed that mangrove soils are exposed 50% of the time
694 (Rosentreter et al., 2018). However, this assumption was not valid for any sampling site
695 of M2 or the upper intertidal zones of M1 and M3 (both showing >90 % exposed time),
696 suggesting that more careful consideration on exposure time is needed.

697 Variable subaerial exposure time along the intertidal zone, attributed to local
698 topography and tidal regime, has been rarely considered in estimates of GHG fluxes in

699 mangroves (*e.g.*, Sotomayor et al., 1994). By upscaling the medians of hourly soil-air flux
700 rates only to the annual exposed period, encompassing lower and upper intertidal zones
701 during summer and winter seasons, we can provide first-order estimates of CO_2 versus
702 CH_4 efflux ~507 versus 0.7, 965 versus 0.7, and 1512 versus 0.8 g C m^{-2} yr^{-1} in M1, M2,
703 and M3, respectively. Accordingly, the longer exposure time over the year contributed to
704 still higher GHG emissions from non-flooded soils in the most impacted mangrove (M3)
705 compared to that most pristine (M1).

706

707 **Conclusions**

708 This multi-proxy analysis of OM elementary, isotopic, and molecular compositions
709 confirms increased eutrophication in mangrove soils are associated with greater urban
710 growth along watersheds. Furthermore, the present results indicate a potential link
711 between untreated wastewater inputs and increased CO_2 emissions to the atmosphere,
712 suggesting a potential loss of blue C from algae or plants from mangrove soils. Hence,
713 our hypothesis was confirmed for CO_2, as indicated by an increased presence of sewage
714 (*e.g.*, higher $\delta^{15}N$, and P, degraded sterols, and coprostanol) and phytoplankton (*e.g.*,
715 lower $\delta^{13}C$ and C:N), which were associated with higher efflux of this gas, independent
716 of intertidal zone or season. However, CH_4 emissions did not increase in mangrove soils
717 surrounded by more urban areas. Soil-air fluxes of this gas varied significantly between
718 intertidal zones and seasons, likely due to the overall low rates associated with high peaks,
719 which were in turn influenced by a greater contribution of labile algal OM seaward and
720 increased freshwater discharges during the rainy summer. Indeed, annual estimates of
721 GHG emissions from exposed mangrove soils after integrating variable exposure times
722 over the tidal regime here may be more realistic, compared to the common assumption
723 that any sampling site in the intertidal zone is flooded for half of the year. Despite this

high complexity of natural and anthropogenic drivers of CO_2 and CH_4 efflux, the greater contribution of OM from algal and sewage sources with coastal eutrophication was generally associated with increased global warming potentials (i.e., carbon emissions to the atmosphere). Our findings support that the control of water pollution and mangrove conservation efforts are critical to climate mitigation for a more sustainable future.

Acknowledgment

This work was supported by the Brazilian National Council for Scientific and Technological Development (CNPq no. 314995/2020-0), the Carlos Chagas Filho Foundation for Research Support of the State of Rio de Janeiro (FAPERJ no. E–26/203.304/2017), the Coordination for the Improvement of Higher Education Personnel (CAPES, Finance Code 001 and the internalization program PRINTCAPES/UFF FEEDBACKS no. 99997.310301/2018-00), the French CNRS-INSU LEFE program and the France-Brazil International Research Project VELITROP (Vulnerability of Tropical Littoral Ecosystem facing eutrophication) funded by the CNRS-INEE, France. HM was the recipient of CNPq Research Productivity and FAPERJ Rio de Janeiro State Scientist grants. The authors are also grateful for the support from the Multi-user Facility for Gas, Water, and Sediment Geochemistry at the Fluminense Federal University (GAS-UFF).

References

Abril, G., Cotovicz Jr, L.C., Nepomuceno, A.M., Erbas, T., Costa, S., Ramos, V.V., Moser, G., Fernandes, A., Negri, E., Knoppers, B.A., Brandini, N., Machado, W., Bernardes, M., Vantrepotte, V., 2022. Spreading eutrophication and changing CO2 fluxes in the tropical coastal ocean: a few lessons from Rio de Janeiro. Arquivos de Ciências do Mar 461–476. https://doi.org/10.32360/78518

Alongi, D., 2009. The Energetics of Mangrove Forests, 1st ed. Springer Netherlands, Dordrecht. https://doi.org/10.1007/978-1-4020-4271-3

Alongi, D.M., Tirendi, F., Dixon, P., Trott, L.A., Brunskill, G.J., 1999. Mineralization of Organic Matter in Intertidal Sediments of a Tropical Semi-enclosed Delta. Estuarine, Coastal and Shelf Science 48, 451–467.

https://doi.org/https://doi.org/10.1006/ecss.1998.0465
Amador, E. da S., 2013. Baía de Guanabara: Ocupação Histórica e Avaliação Ambiental, 1st ed. Interciência.
APHA, AWWA, WEF, 2012. Standard Methods for examination of water and wastewater, 22nd ed. American Public Health Association, Washington.
Araujo, M.P., Costa, T.L.F. da, Carreira, R. da S., 2011. Esterois como indicadores do acúmulo de esgotos domésticos em sedimentos de um sistema estuarino-lagunar tropical (Mundaú-Manguaba, AL). Química Nova 34, 64–70.
Barcellos, D., Queiroz, H.M., Nóbrega, G.N., de Oliveira Filho, R.L., Santaella, S.T., Otero, X.L., Ferreira, T.O., 2019. Phosphorus enriched effluents increase eutrophication risks for mangrove systems in northeastern Brazil. Marine Pollution Bulletin 142, 58–63. https://doi.org/10.1016/j.marpolbul.2019.03.031
Barros, G.V., Martinelli, L.A., Oliveira Novais, T.M., Ometto, J.P.H.B., Zuppi, G.M., 2010. Stable isotopes of bulk organic matter to trace carbon and nitrogen dynamics in an estuarine ecosystem in Babitonga Bay (Santa Catarina, Brazil). Science of the Total Environment 408, 2226–2232. https://doi.org/10.1016/j.scitotenv.2010.01.060
Boehm, P.D., Requejo, A.G., 1986. Overview of the recent sediment hydrocarbon geochemistry of Atlantic and Gulf Coast outer continental shelf environments. Estuarine, Coastal and Shelf Science 23, 29–58. https://doi.org/https://doi.org/10.1016/0272-7714(86)90084-3
Borges, H.V., Nittrouer, C.A., 2016. SEDIMENT ACCUMULATION IN SEPETIBA BAY (BRAZIL) DURING THE HOLOCENE: A REFLEX OF THE HUMAN INFLUENCE. Journal of Sedimentary Environments 1. https://doi.org/10.12957/jse.2016.21868
Bourbonniere, R.A., Meyers, P.A., 1996. Sedimentary geolipid records of historical changes in the watersheds and productivities of Lakes Ontario and Erie. Limnology and Oceanography 41, 352–359.
Brandini, F., Michelazzo, L.S., Freitas, G.R., Campos, G., Chuqui, M., Jovane, L., 2019. Carbon Flow for Plankton Metabolism of Saco do Mamanguá Ría, Bay of Ilha Grande, a Subtropical Coastal Environment in the South Brazil Bight. Front Mar Sci 6. https://doi.org/10.3389/fmars.2019.00584
Breitburg, D., Levin, L.A., Oschlies, A., Grégoire, M., Chavez, F.P., Conley, D.J., Garçon, V., Gilbert, D., Gutiérrez, D., Isensee, K., Jacinto, G.S., Limburg, K.E., Montes, I., Naqvi, S.W.A., Pitcher, G.C., Rabalais, N.N., Roman, M.R., Rose, K.A., Seibel, B.A., Telszewski, M., Yasuhara, M., Zhang, J., 2018. Declining oxygen in the global ocean and coastal waters. Science (1979) 359, eaam7240. https://doi.org/10.1126/science.aam7240
Canuel, E.A., Freeman, K.H., Wakeham, S.G., 1997. Isotopic compositions of lipid biomarker compounds in estuarine plants and surface sediments. Limnology and Oceanography 42, 1570–1583. https://doi.org/10.4319/lo.1997.42.7.1570
Carreira, R., Wagener, A. de L.R., Fileman, T., Readman, J.W., 2001. Distribuição de coprostanol (5beta(H)-colestan-3beta-ol) em sedimentos superficiais da Baía de Guanabara: indicador da poluição recente por esgotos domésticos. Química Nova 24. https://doi.org/10.1590/S0100-40422001000100008
Carreira, R.S., Ribeiro, P. v., Silva, C.E.M., Farias, C.O., 2009. Hidrocarbonetos e esterois como indicadores de fontes e destino de matéria orgânica em sedimentos da Baía de Sepetiba, Rio de Janeiro. Química Nova 32. https://doi.org/10.1590/S0100-40422009000700023
Chen, G.C., Tam, N.F.Y., Wong, Y.S., Ye, Y., 2011. Effect of wastewater discharge on greenhouse gas fluxes from mangrove soils. Atmospheric Environment 45, 1110–1115. https://doi.org/10.1016/j.atmosenv.2010.11.034

Chen, G.C., Tam, N.F.Y., Ye, Y., 2010. Summer fluxes of atmospheric greenhouse gases N2O, CH4 and CO2 from mangrove soil in South China. Science of the Total Environment 408, 2761–2767. https://doi.org/10.1016/j.scitotenv.2010.03.007

Chen, G.C., Tam, N.F.Y., Ye, Y., 2012. Spatial and seasonal variations of atmospheric N2O and CO2 fluxes from a subtropical mangrove swamp and their relationships with soil characteristics. Soil Biology and Biochemistry 48, 175–181. https://doi.org/10.1016/j.soilbio.2012.01.029

Clark Jr., R.C., Blumer, M., 1967. DISTRIBUTION OF n-PARAFFINS IN MARINE ORGANISMS AND SEDIMENT1. Limnology and Oceanography 12, 79–87. https://doi.org/https://doi.org/10.4319/lo.1967.12.1.0079

Copeland, G., Monteiro, T., Couch, S., Borthwick, A., 2003. Water quality in Sepetiba Bay, Brazil. Marine Environmental Research 55, 385–408. https://doi.org/10.1016/S0141-1136(02)00289-1

Das, S., Ganguly, D., Chakraborty, S., Mukherjee, A., Kumar De, T., 2018. Methane flux dynamics in relation to methanogenic and methanotrophic populations in the soil of Indian Sundarban mangroves. Marine Ecology 39, e12493.

Dell'Anno, A., Mei, M.L., Pusceddu, A., Danovaro, R., 2002. Assessing the trophic state and eutrophication of coastal marine systems: a new approach based on the biochemical composition of sediment organic matter. Marine Pollution Bulletin 44, 611–622. https://doi.org/10.1016/S0025-326X(01)00302-2

dos Reis Souza, M.R., Santos, E., Suzarte, J.S., do Carmo, L.O., Soares, L.S., Santos, L.G.G.V., Júnior, A.R.V., Krause, L.C., Frena, M., Damasceno, F.C., Huang, Y., da Rosa Alexandre, M., 2020. The impact of anthropogenic activity at the tropical Sergipe-Poxim estuarine system, Northeast Brazil: Fecal indicators. Marine Pollution Bulletin 154, 111067. https://doi.org/10.1016/j.marpolbul.2020.111067

Drake, T.W., Podgorski, D.C., Dinga, B., Chanton, J.P., Six, J., Spencer, R.G.M., 2020. Land-use controls on carbon biogeochemistry in lowland streams of the Congo Basin. Global Change Biology 26, 1374–1389. https://doi.org/https://doi.org/10.1111/gcb.14889

Eglinton, G., Gonzalez, A.G., Hamilton, R.J., Raphael, R.A., 1962. Hydrocarbon constituents of the wax coatings of plant leaves: A taxonomic survey. Phytochemistry 1, 89–102. https://doi.org/https://doi.org/10.1016/S0031-9422(00)88006-1

Faria, M. de M., Sanchez, B.A., 2001. Geochemistry and mineralogy of recent sediments of Guanabara Bay (NE sector) and its major rivers - Rio de Janeiro State - Brazil. Anais da Academia Brasileira de Ciências 73, 121–133. https://doi.org/10.1590/S0001-37652001000100010

Fistarol, G.O., Coutinho, F.H., Moreira, A.P.B., Venas, T., Cánovas, A., de Paula, S.E.M., Coutinho, R., de Moura, R.L., Valentin, J.L., Tenenbaum, D.R., Paranhos, R., do Valle, R. de A.B., Vicente, A.C.P., Amado Filho, G.M., Pereira, R.C., Kruger, R., Rezende, C.E., Thompson, C.C., Salomon, P.S., Thompson, F.L., 2015. Environmental and Sanitary Conditions of Guanabara Bay, Rio de Janeiro. Frontiers in Microbiology 6. https://doi.org/10.3389/fmicb.2015.01232

Folk, R.L., Ward, W.C., 1957. Brazos River bar [Texas]; a study in the significance of grain size parameters. Journal of Sedimentary Research 27, 3–26. https://doi.org/10.1306/74D70646-2B21-11D7-8648000102C1865D

Franco, A.S., 1997. Marés, Fundamentos, in: Navegação, D. de H. e (Ed.), Análise e Previsão. Niterói, RJ.

Frena, M., Souza, M.R.R., Damasceno, F.C., Madureira, L.A.S., Alexandre, M.R., 2016. Evaluation of anthropogenic contamination using sterol markers in a tropical estuarine system of northeast Brazil. Marine Pollution Bulletin 109, 619–623.

https://doi.org/10.1016/j.marpolbul.2016.05.022
García, L. V., 2004. Escaping the Bonferroni iron claw in ecological studies. Oikos 105, 657–663. https://doi.org/10.1111/j.0030-1299.2004.13046.x
Gearing, P., Gearing, J.N., Lytle, T.F., Lytle, J.S., 1976. Hydrocarbons in 60 northeast Gulf of Mexico shelf sediments: a preliminary survey. Geochimica et Cosmochimica Acta 40, 1005–1017. https://doi.org/10.1016/0016-7037(76)90043-0
Gontikaki, E., Thornton, B., Cornulier, T., Witte, U., 2015. Occurrence of Priming in the Degradation of Lignocellulose in Marine Sediments. PLOS ONE 10. https://doi.org/10.1371/journal.pone.0143917
González-Oreja, J.A., Saiz-Salinas, J.I., 1998. Short-term spatio-temporal changes in urban pollution by means of faecal sterols analysis. Marine Pollution Bulletin 36, 868–875. https://doi.org/10.1016/S0025-326X(98)00037-X
Grasshoff, K., Ehrardt, M., Kremling, K., 1999. Methods of Seawater Analysis. Wiley. https://doi.org/10.1002/9783527613984
Grimalt, J.O., Fernandez, P., Bayona, J.M., Albaiges, J., 1990. Assessment of fecal sterols and ketones as indicators of urban sewage inputs to coastal waters. Environmental Science & Technology 24, 357–363. https://doi.org/10.1021/es00073a011
Gritcan, I., Duxbury, M., Leuzinger, S., Alfaro, A.C., 2016. Leaf stable isotope and nutrient status of temperate mangroves as ecological indicators to assess anthropogenic activity and recovery from eutrophication. Front Plant Sci 7, 1922.
Guenet, B., Neill, C., Bardoux, G., Abbadie, L., 2010. Is there a linear relationship between priming effect intensity and the amount of organic matter input? Applied Soil Ecology 46, 436–442. https://doi.org/10.1016/j.apsoil.2010.09.006
Guoying, S., Shanfa, F., Dehan, L., Nengxian, S., Hongming, Z., 1980. The geochemistry of n-alkanes with an even-odd predominance in the Tertiary Shahejie Formation of northern China. Physics and Chemistry of the Earth 12, 115–121. https://doi.org/10.1016/0079-1946(79)90093-4
Häder, D.-P., Banaszak, A.T., Villafañe, V.E., Narvarte, M.A., González, R.A., Helbling, E.W., 2020. Anthropogenic pollution of aquatic ecosystems: Emerging problems with global implications. Science of The Total Environment 713. https://doi.org/10.1016/j.scitotenv.2020.136586
Hamilton, S.E., Friess, D.A., 2018. Global carbon stocks and potential emissions due to mangrove deforestation from 2000 to 2012. Nature Climate Change 8, 240–244. https://doi.org/10.1038/s41558-018-0090-4
Hutchinson, G.L., Livingston, G.P., 2001. Vents and seals in non-steady-state chambers used for measuring gas exchange between soil and the atmosphere. European Journal of Soil Science 52, 675–682. https://doi.org/10.1046/j.1365-2389.2001.00415.x
IBGE, 2010. 2010 Census - Brazilian Institute of Geography and Statistics [WWW Document]. URL https://cidades.ibge.gov.br/brasil/rj/panorama
Isobe, K.O., Tarao, M., Zakaria, M.P., Chiem, N.H., Minh, L.Y., Takada, H., 2002. Quantitative Application of Fecal Sterols Using Gas Chromatography−Mass Spectrometry To Investigate Fecal Pollution in Tropical Waters: Western Malaysia and Mekong Delta, Vietnam. Environmental Science & Technology 36, 4497–4507. https://doi.org/10.1021/es020556h
Jacotot, A., Marchand, C., Allenbach, M., 2018. Tidal variability of CO2 and CH4 emissions from the water column within a Rhizophora mangrove forest (New Caledonia). Science of the Total Environment 631–632, 334–340. https://doi.org/10.1016/j.scitotenv.2018.03.006
Jacotot, A., Marchand, C., Allenbach, M., 2019. Biofilm and temperature controls on greenhouse gas (CO2 and CH4) emissions from a Rhizophora mangrove soil (New Caledonia). Science of The Total Environment 650.

907 https://doi.org/10.1016/j.scitotenv.2018.09.093
908 Jeng, W.L., 2006. Higher plant n-alkane average chain length as an indicator of
909 petrogenic hydrocarbon contamination in marine sediments. Marine Chemistry 102,
910 242–251. https://doi.org/10.1016/j.marchem.2006.05.001
911 Jiao, N., Wang, H., Xu, G., Aricò, S., 2018. Blue carbon on the rise: Challenges and
912 opportunities. National Science Review 5, 464–468.
913 Kabwe, L.K., Hendry, M.J., Wilson, G.W., Lawrence, J.R., 2002. Quantifying CO2
914 fluxes from soil surfaces to the atmosphere. Journal of Hydrology 260, 1–14.
915 https://doi.org/10.1016/S0022-1694(01)00601-1
916 Keller, M., Weitz, A.M., Bryan, B., Rivera, M.M., Silver, W.L., 2000. Soil-atmosphere
917 nitrogen oxide fluxes: Effects of root disturbance. Journal of Geophysical Research:
918 Atmospheres 105, 17693–17698. https://doi.org/10.1029/2000JD900068
919 Keuskamp, J.A., Hefting, M.M., Dingemans, B.J.J., Verhoeven, J.T.A., Feller, I.C., 2015.
920 Effects of nutrient enrichment on mangrove leaf litter decomposition. Science of The
921 Total Environment 508, 402–410. https://doi.org/10.1016/j.scitotenv.2014.11.092
922 King, G.M., 1984. Utilization of hydrogen, acetate, and “noncompetitive”; substrates by
923 methanogenic bacteria in marine sediments. Geomicrobiology Journal 3, 275–306.
924 Konnerup, D., Betancourt-Portela, J.M., Villamil, C., Parra, J.P., 2014. Nitrous oxide and
925 methane emissions from the restored mangrove ecosystem of the Ciénaga Grande de
926 Santa Marta, Colombia. Estuarine, Coastal and Shelf Science 140, 43–51.
927 https://doi.org/10.1016/j.ecss.2014.01.006
928 Kreuzwieser, J., Buchholz, J., Rennenberg, H., 2003. Emission of Methane and Nitrous
929 Oxide by Australian Mangrove Ecosystems. Plant Biology 5.
930 https://doi.org/10.1055/s-2003-42712
931 Kristensen, E., Alongi, D.M., 2006. Control by fiddler crabs (Uca vocans) and plant roots
932 (Avicennia marina) on carbon, iron, and sulfur biogeochemistry in mangrove
933 sediment. Limnology and Oceanography 51.
934 https://doi.org/10.4319/lo.2006.51.4.1557
935 Kristensen, E., Bouillon, S., Dittmar, T., Marchand, C., 2008a. Organic carbon dynamics
936 in mangrove ecosystems: A review. Aquatic Botany 89, 201–219.
937 https://doi.org/10.1016/j.aquabot.2007.12.005
938 Kristensen, E., Connolly, R.M., Otero, X.L., Marchand, C., Ferreira, T.O., Rivera-
939 Monroy, V.H., 2017. Biogeochemical Cycles: Global Approaches and Perspectives,
940 in: Mangrove Ecosystems: A Global Biogeographic Perspective. Springer
941 International Publishing, Cham. https://doi.org/10.1007/978-3-319-62206-4_6
942 Kristensen, E., Flindt, M.R., Ulomi, S., Borges, A. v., Abril, G., Bouillon, S., 2008b.
943 Emission of CO2 and CH4 to the atmosphere by sediments and open waters in two
944 Tanzanian mangrove forests. Marine Ecology Progress Series 370, 53–67.
945 https://doi.org/10.3354/meps07642
946 Kumar, M., Boski, T., Lima-Filho, F.P., Bezerra, F.H.R., González -Vila, F.J., Alam
947 Bhuiyan, M.K., González-Pérez, J.A., 2019. Biomarkers as indicators of
948 sedimentary organic matter sources and early diagenetic transformation of
949 pentacyclic triterpenoids in a tropical mangrove ecosystem. Estuarine, Coastal and
950 Shelf Science 229, 106403. https://doi.org/10.1016/j.ecss.2019.106403
951 Lam, S.Y.W., Chen, Y.-Q., 2001. Ground-Based Positioning Techniques, in:
952 Geographical Data Acquisition. Springer Vienna, Vienna, pp. 85–97.
953 https://doi.org/10.1007/978-3-7091-6183-8_6
954 Lamb, A.L., Wilson, G.P., Leng, M.J., 2006. A review of coastal palaeoclimate and
955 relative sea-level reconstructions using δ13C and C/N ratios in organic material.
956 Earth-Science Reviews 75, 29–57.
957 Lemley, D.A., Adams, J.B., Taljaard, S., Strydom, N.A., 2015. Towards the classification

of eutrophic condition in estuaries. Estuarine, Coastal and Shelf Science 164, 221–232. https://doi.org/10.1016/j.ecss.2015.07.033
Leng, M.J., Lewis, J.P., 2017. C/N ratios and Carbon Isotope Composition of Organic Matter in Estuarine Environments. pp. 213–237. https://doi.org/10.1007/978-94-024-0990-1_9
Liu, S., Trevathan-Tackett, S.M., Ewers Lewis, C.J., Huang, X., Macreadie, P.I., 2020. Macroalgal Blooms Trigger the Breakdown of Seagrass Blue Carbon. Environmental Science & Technology 54, 14750–14760. https://doi.org/10.1021/acs.est.0c03720
Machiwa, J.F., 2000. d13C Signatures of Flora, Macrofauna and Sediment of a Mangrove Forest Partly Affected by Sewage Wastes. Tanzania Journal of Science 26, 15–28.
Mannino, A., Harvey, H.R., 1999. Lipid composition in particulate and dissolved organic matter in the Delaware Estuary: sources and diagenetic patterns. Geochimica et Cosmochimica Acta 63, 2219–2235. https://doi.org/https://doi.org/10.1016/S0016-7037(99)00128-3
Marins, R. V., Machado, W., Paraquetti, H.H.M., Bidone, E.D., Lacerda, L.D., Molisani, M.M., 2004. Environmental changes in Sepetiba Bay, SE Brazil. Regional Environmental Change 4, 17–27. https://doi.org/10.1007/s10113-003-0060-9
Marotta, H., Duarte, C.M., Guimarães-Souza, B.A., Enrich-Prast, A., 2012. Synergistic control of CO2 emissions by fish and nutrients in a humic tropical lake. Oecologia 168, 839–847. https://doi.org/10.1007/s00442-011-2131-9
Martens, C.S., Berner, R.A., 1974. Methane Production in the Interstitial Waters of Sulfate-Depleted Marine Sediments. Science (1979) 185, 1167–1169. https://doi.org/10.1126/science.185.4157.1167
Martin, R.M., Wigand, C., Oczkowski, A., Hanson, A., Balogh, S., Branoff, B., Santos, E., Huertas, E., 2020. Greenhouse Gas Fluxes of Mangrove Soils and Adjacent Coastal Waters in an Urban, Subtropical Estuary. Wetlands 40. https://doi.org/10.1007/s13157-020-01300-w
McCaffrey, M.A., 1990. Sedimentary lipids as indicators of depositional conditions in the coastal Peruvian upwelling regime. https://doi.org/10.1575/1912/5428
McCalley, D. V, Cooke, M., Nickless, G., 1981. Effect of sewage treatment on faecal sterols. Water Research 15, 1019–1025. https://doi.org/https://doi.org/10.1016/0043-1354(81)90211-6
Meyers, P.A., 1994. Preservation of elemental and isotopic source identification of sedimentary organic matter. Chemical Geology 114, 289–302. https://doi.org/https://doi.org/10.1016/0009-2541(94)90059-0
Molisani, M.M., Kjerfve, B., Silva, A.P., Lacerda, L.D., 2006. Water discharge and sediment load to Sepetiba Bay from an anthropogenically-altered drainage basin, SE Brazil. Journal of Hydrology 331, 425–433. https://doi.org/10.1016/j.jhydrol.2006.05.038
Moser, K., Ahn, C., Noe, G., 2007. Characterization of microtopography and its influence on vegetation patterns in created wetlands. Wetlands 27, 1081–1097.
Mudge, S.M., Bebianno, M.J., 1997. Sewage contamination following an accidental spillage in the Ria Formosa, Portugal. Marine Pollution Bulletin 34, 163–170. https://doi.org/https://doi.org/10.1016/S0025-326X(96)00082-3
Mudge, S.M., Lintern, D.G., 1999. Comparison of Sterol Biomarkers for Sewage with other Measures in Victoria Harbour, B.C., Canada. Estuarine, Coastal and Shelf Science 48, 27–38. https://doi.org/10.1006/ecss.1999.0406
Mudge, S.M., Seguel, C.G., 1999. Organic Contamination of San Vicente Bay, Chile. Marine Pollution Bulletin 38, 1011–1021. https://doi.org/https://doi.org/10.1016/S0025-326X(99)00132-0

1009 Muniz, P., Pires-Vanin, A.M.S., Martins, C.C., Montone, R.C., Bícego, M.C., 2006.
1010 Trace metals and organic compounds in the benthic environment of a subtropical
1011 embayment (Ubatuba Bay, Brazil). Marine Pollution Bulletin 52, 1098–1105.
1012 https://doi.org/10.1016/j.marpolbul.2006.05.014
1013 Nes, W.R., 1974. Role of sterols in membranes. Lipids 9, 596–612.
1014 https://doi.org/10.1007/BF02532509
1015 Nishigima, F.N., Weber, R.R., Bicego, M.C., 2001. Aliphatic and aromatic hydrocarbons
1016 in sediments of Santos and Cananéia, SP, Brazil. Marine Pollution Bulletin 42,
1017 1064–1072. https://doi.org/10.1016/S0025-326X(01)00072-8
1018 Nishimura, M., Koyama, T., 1976. Stenols and stanols in lake sediments and diatoms.
1019 Chemical Geology 17, 229–239. https://doi.org/https://doi.org/10.1016/0009-
1020 2541(76)90037-1
1021 Nishimura, M., Koyama, T., 1977. The occurrence of stanols in various living organisms
1022 and the behavior of sterols in contemporary sediments. Geochimica et
1023 Cosmochimica Acta 41, 379–385. https://doi.org/https://doi.org/10.1016/0016-
1024 7037(77)90265-4
1025 Nixon, S.W., 1995. Coastal marine eutrophication: A definition, social causes, and future
1026 concerns. Ophelia 41, 199–219. https://doi.org/10.1080/00785236.1995.10422044
1027 Nóbrega, G.N., Ferreira, T.O., Siqueira Neto, M., Queiroz, H.M., Artur, A.G., Mendonça,
1028 E.D.S., Silva, E.D.O., Otero, X.L., 2016. Edaphic factors controlling summer (rainy
1029 season) greenhouse gas emissions (CO2 and CH4) from semiarid mangrove soils
1030 (NE-Brazil). Science of the Total Environment 542, 685–693.
1031 https://doi.org/10.1016/j.scitotenv.2015.10.108
1032 Ouyang, X., Lee, S.Y., Connolly, R.M., 2016. Structural equation modelling reveals
1033 factors regulating surface sediment organic carbon content and CO2 efflux in a
1034 subtropical mangrove. Science of the Total Environment 578, 513–522.
1035 https://doi.org/http://dx.doi.org/10.1016/j.scitotenv.2016.10.218
1036 Palacios, M.M., Trevathan-Tackett, S.M., Malerba, M.E., Macreadie, P.I., 2021. Effects
1037 of a nutrient enrichment pulse on blue carbon ecosystems. Marine Pollution Bulletin
1038 165, 112024. https://doi.org/10.1016/j.marpolbul.2021.112024
1039 Pérez, A., Machado, W., Gutierrez, D., Smoak, J.M., Breithaupt, J.L., Saldarriaga, M.S.,
1040 Sanders, L., Marotta, H., Sanders, C.J., 2020. Carbon and nutrient accumulation in
1041 mangrove sediments affected by multiple environmental changes. Journal of Soils
1042 and Sediments 20. https://doi.org/10.1007/s11368-020-02612-4
1043 Pratt, C., Warnken, J., Leeming, R., Arthur, M.J., Grice, D.I., 2008. Degradation and
1044 responses of coprostanol and selected sterol biomarkers in sediments to a simulated
1045 major sewage pollution event: A microcosm experiment under sub-tropical estuarine
1046 conditions. Organic Geochemistry 39, 353–369.
1047 https://doi.org/https://doi.org/10.1016/j.orggeochem.2007.06.009
1048 Purvaja, R., Ramesh, R., 2001. Natural and anthropogenic methane emission from coastal
1049 wetlands of South India. Environmental Management 27, 547–557.
1050 Queiroz, H.M., Ferreira, T.O., Taniguchi, C.A.K., Barcellos, D., do Nascimento, J.C.,
1051 Nóbrega, G.N., Otero, X.L., Artur, A.G., 2020. Nitrogen mineralization and
1052 eutrophication risks in mangroves receiving shrimp farming effluents.
1053 Environmental Science and Pollution Research 27, 34941–34950.
1054 https://doi.org/10.1007/s11356-020-09720-1
1055 Rochette, P., Hutchinson, G.L., 2015. Measurement of Soil Respiration in situ: Chamber
1056 Techniques. pp. 247–286. https://doi.org/10.2134/agronmonogr47.c12
1057 Rosentreter, Judith A, Maher, D.T., Erler, D. V, Murray, R.H., Eyre, B.D., 2018. Methane
1058 emissions partially offset “blue carbon” burial in mangroves. Sci Adv 4, eaao4985.
1059 Rosentreter, Judith A., Maher, D.T., Erler, D. v., Murray, R.H., Eyre, B.D., 2018.

Methane emissions partially offset “blue carbon” burial in mangroves. Science Advances 4. https://doi.org/10.1126/sciadv.aao4985
Sanders, C.J., Eyre, B.D., Santos, I.R., Machado, W., Luiz-Silva, W., Smoak, J.M., Breithaupt, J.L., Ketterer, M.E., Sanders, L., Marotta, H., Silva-Filho, E., 2014. Elevated rates of organic carbon, nitrogen, and phosphorus accumulation in a highly impacted mangrove wetland. Geophysical Research Letters 41. https://doi.org/10.1002/2014GL059789
Sanders, C.J., Smoak, J.M., Naidu, A.S., Araripe, D.R., Sanders, L.M., Patchineelam, S.R., 2010a. Mangrove forest sedimentation and its reference to sea level rise, Cananeia, Brazil. Environmental Earth Sciences 60, 1291–1301.
Sanders, C.J., Smoak, J.M., Naidu, A.S., Sanders, L.M., Patchineelam, S.R., 2010b. Organic carbon burial in a mangrove forest, margin and intertidal mud flat. Estuarine, Coastal and Shelf Science 90, 168–172.
Santos, E.S., Carreira, R. da S., Knoppers, B.A., 2008. Sedimentary sterols as indicators of environmental conditions in Southeastern Guanabara Bay, Brazil. Brazilian Journal of Oceanography 56, 97–113.
Schaeffer-Novelli, Y., Cintrón-Molero, G., Soares, M.L.G., De-Rosa, T., 2000. Brazilian mangroves. Aquatic Ecosystem Health & Management 3, 561–570. https://doi.org/10.1080/14634980008650693
Schumacher, B.A., 2002. METHODS FOR THE DETERMINATION OF TOTAL ORGANIC CARBON (TOC) IN SOILS AND SEDIMENTS. Las Vegas.
Servais, S., Kominoski, J.S., Davis, S.E., Gaiser, E.E., Pachón, J., Troxler, T.G., 2019. Effects of Nutrient-Limitation on Disturbance Recovery in Experimental Mangrove Wetlands. Wetlands 39, 337–347. https://doi.org/10.1007/s13157-018-1100-z
Sherman, R.E., Fahey, T.J., Howarth, R.W., 1998. Soil-plant interactions in a neotropical mangrove forest: iron, phosphorus and sulfur dynamics. Oecologia 115, 553–563.
Sotomayor, D., Corredor, J.E., Morell, J.M., 1994. Methane Flux from Mangrove Sediments along the Southwestern Coast of Puerto Rico. Estuaries 17. https://doi.org/10.2307/1352563
Steinhauer, M.S., Boehm, P.D., 1992. The composition and distribution of saturated and aromatic hydrocarbons in nearshore sediments, river sediments, and coastal peat of the Alaskan Beaufort Sea: Implications for detecting anthropogenic hydrocarbon inputs. Marine Environmental Research 33, 223–253. https://doi.org/10.1016/0141-1136(92)90140-H
Thomazelli, F.F., 2010. Composição da matéria orgânica no gradiente estuarino da Baía de Sepetiba/RJ. Universidade Federal Fluminense.
Tomotsune, M., Arai, H., Yoshitake, S., Kida, M., Fujitake, N., Kinjo, K., Ohtsuka, T., 2020. Effect of Crab Burrows on CO 2 Flux from the Sediment Surface to the Atmosphere in a Subtropical Mangrove Forest on Ishigaki Island, Southwestern Japan. Estuaries and Coasts 43, 102–110.
van Nugteren, P., Moodley, L., Brummer, G.-J., Heip, C.H.R., Herman, P.M.J., Middelburg, J.J., 2009. Seafloor ecosystem functioning: the importance of organic matter priming. Marine Biology 156, 2277–2287. https://doi.org/10.1007/s00227-009-1255-5
Verhoeven, J.T.A., Laanbroek, H.J., Rains, M.C., Whigham, D.F., 2014. Effects of increased summer flooding on nitrogen dynamics in impounded mangroves. Journal of Environmental Management 139, 217–226. https://doi.org/10.1016/j.jenvman.2014.02.035
Vizza, C., West, W.E., Jones, S.E., Hart, J.A., Lamberti, G.A., 2017. Regulators of coastal wetland methane production and responses to simulated global change. Biogeosciences 14, 431–446.

Wakeham, S.G., Canuel, E.A., 1988. Organic geochemistry of particulate matter in the eastern tropical North Pacific Ocean: Implications for particle dynamics. Journal of Marine Research 46, 183–213. https://doi.org/10.1357/002224088785113748

Wang, X.-C., Chen, R.F., Berry, A., 2003. Sources and preservation of organic matter in Plum Island salt marsh sediments (MA, USA): long-chain n-alkanes and stable carbon isotope compositions. Estuarine, Coastal and Shelf Science 58, 917–928. https://doi.org/https://doi.org/10.1016/j.ecss.2003.07.006

Wang, X.C., Sun, S., Ma, H.Q., Liu, Y., 2006. Sources and distribution of aliphatic and polyaromatic hydrocarbons in sediments of Jiaozhou Bay, Qingdao, China. Marine Pollution Bulletin 52, 129–138. https://doi.org/10.1016/j.marpolbul.2005.08.010

Wendlandt, W.W.M., 1986. Thermal Analysis. John Wiley, New York.

Wheaton, J.M., Brasington, J., Darby, S.E., Sear, D.A., 2009. Accounting for uncertainty in DEMs from repeat topographic surveys: improved sediment budgets. Earth Surface Processes and Landforms n/a-n/a. https://doi.org/10.1002/esp.1886

Wolters, J.-W., Gillis, L.G., Bouma, T.J., van Katwijk, M.M., Ziegler, A.D., 2016. Land Use Effects on Mangrove Nutrient Status in Phang Nga Bay, Thailand. Land Degradation \& Development 27, 68–76. https://doi.org/https://doi.org/10.1002/ldr.2430

Yang, Z., Song, W., Zhao, Y., Zhou, J., Wang, Z., Luo, Y., Li, Y., Lin, G., 2018. Differential responses of litter decomposition to regional excessive nitrogen input and global warming between two mangrove species. Estuarine, Coastal and Shelf Science 214, 141–148. https://doi.org/10.1016/j.ecss.2018.09.018

Zar, J.H., 1996. Biostatistical analysis, 3rd ed. Prentice Hall., New Jersey.

Zhang, Y., Lu, X., Liu, H., Liu, Q., Yu, D., 2015. Identifying the sources of organic matter in marine and riverine sediments of Bohai Bay and its catchment using carbon and nitrogen stable isotopes. Chinese Journal of Oceanology and Limnology 33, 204–209. https://doi.org/10.1007/s00343-015-4068-z

1139 **Figures**

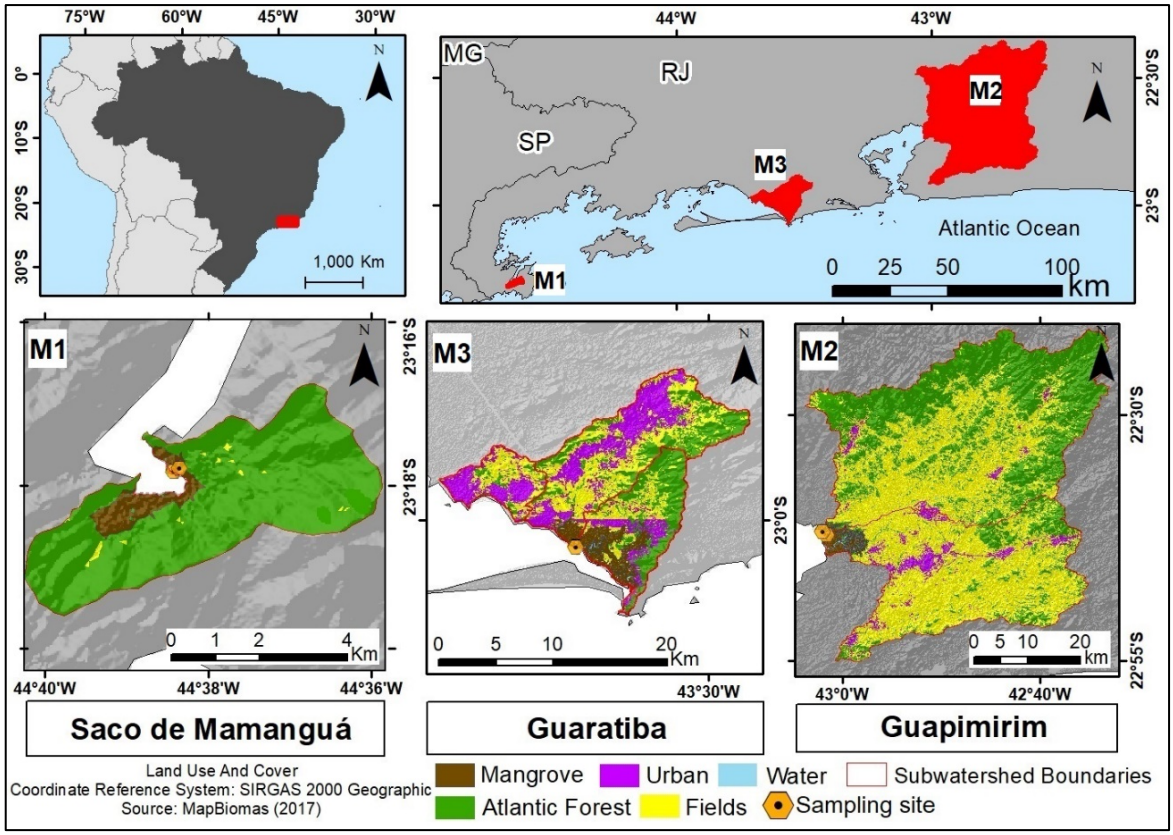

1140

1141 Fig.1. Location of the tree studied mangroves and their respective drainage basins including land
1142 use characteristics. All sites are located within Rio de Janeiro State, southeastern Brazil. Ilha
1143 Grande Bay, the Sepetiba Bay and the Guanabara Bay show Saco de Mamanguá (M1), Guaratiba
1144 (M3) and Guapimirim (M2) mangroves, respectively. Land use and land cover was based on the
1145 MapBiomas dataset (2017), available at https://plataforma.mapbiomas.org/map#coverage.

1146

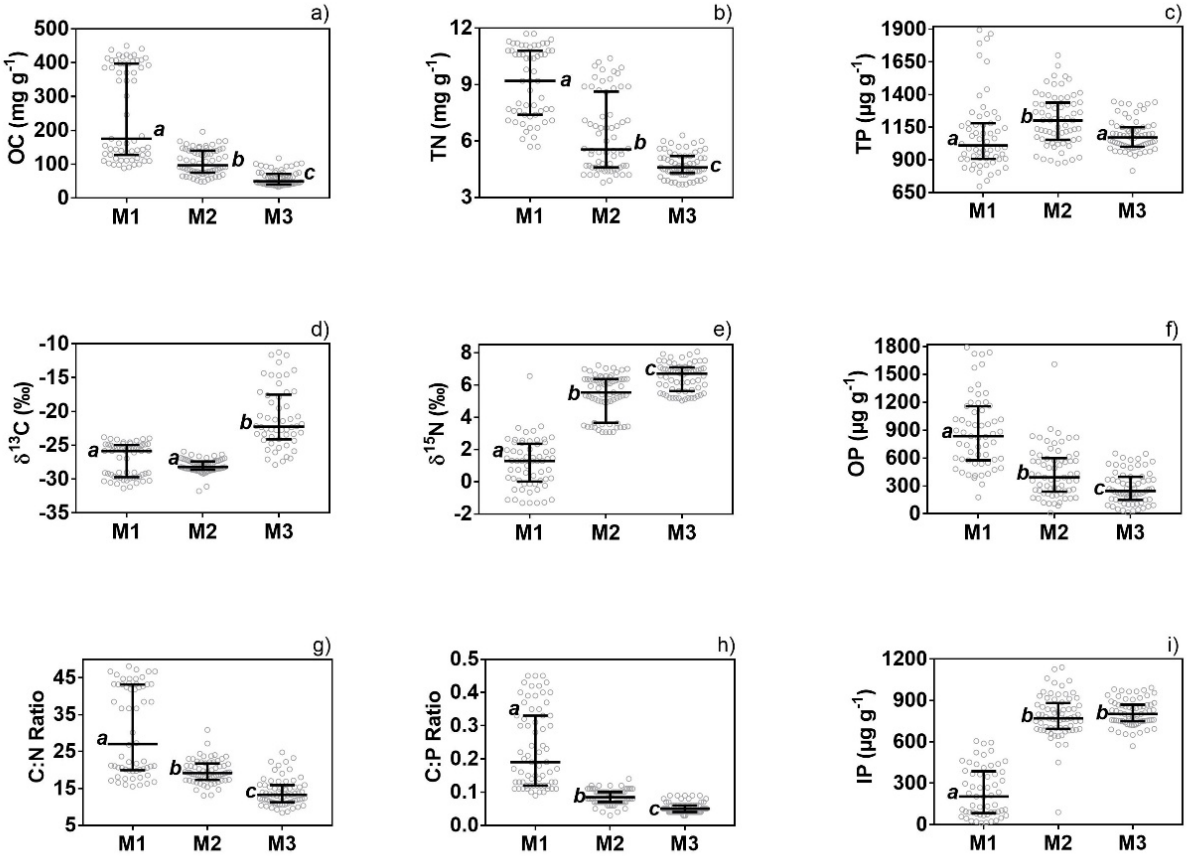

Fig. 2. Spatial comparison of the elementary composition among Mamanguá (M1), Guapimirim (M2) and Guaratiba (M3) mangroves soils (Kruskal Wallis, $p<0,05$), in which a) total organic carbon (OC, mg g^{-1}), b) total nitrogen (TN, mg g^{-1}), c) total phosphorus (TP, µg g^{-1}), d) isotopic ratios of ^{13}C ($\delta^{13}C$, ‰), e) isotopic ratios of ^{15}N ($\delta^{15}N$, ‰), f) organic phosphorus (OP, µg g^{-1}), g) OC to TN ratio (C:N), h) OC to TP ratio (C:P), and i) inorganic phosphorus concentration (IP, µg g^{-1}). Horizontal line represent median, bars represent interquartile range, and different letters represent statistically significant difference.

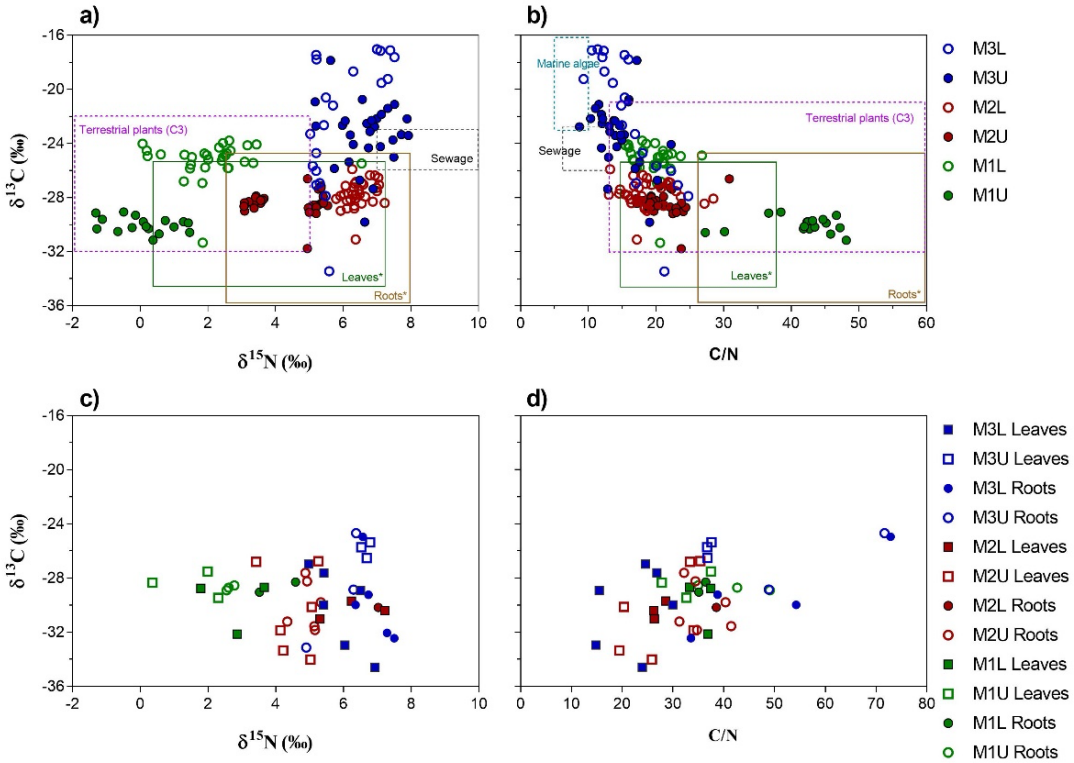

1156

1157 Fig. 3. Relationships between (a) $\delta^{15}N$ and $\delta^{13}C$ in soils, (b) C:N and $\delta^{13}C$ in soils, (c) $\delta^{15}N$ and
1158 $\delta^{13}C$ in leaves and roots, and (d) C:N and $\delta^{13}C$ in leaves and roots of Mamanguá (M1), Guapimirim
1159 (M2), and Guaratiba (M3) mangroves, including upper and lower zones. The ranges of terrestrial
1160 plants, marine algae and freshwater algae are those reported in (Leng and Lewis, 2017). Sewage
1161 range data reported in Barros et al. (2010).

1162

1163

1164

1165

1166

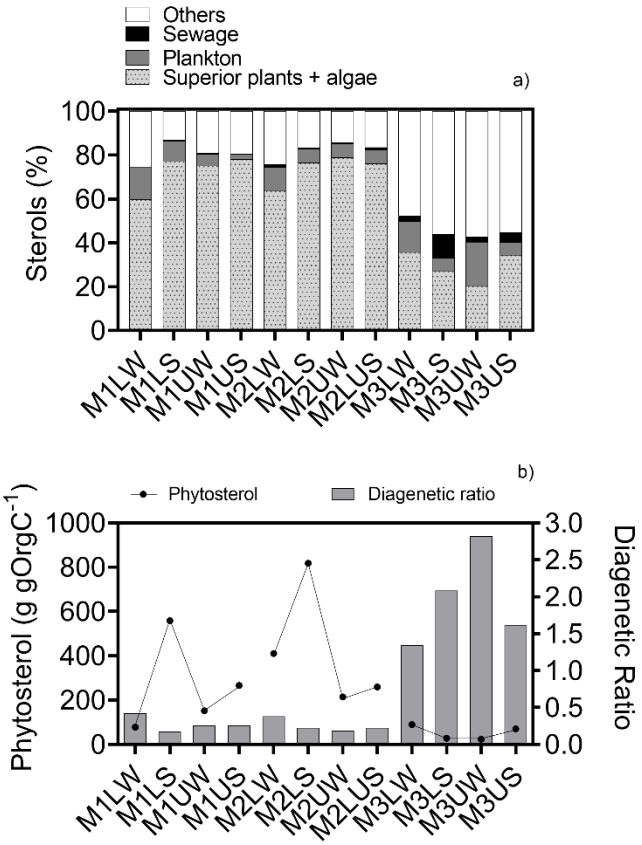

1167

1168 Fig.4. a) Relative contribution of different sources of sterols in soils of upper (U) and lower (L)
1169 zone in Mamanguá (M1), Guapimirim (M2) and Guaratiba (M3) mangroves during winter (W)
1170 and summer (S) periods. Sewage origin identified by the presence of 5β-cholestan-3β-ol
1171 (coprostanol) and 5β-cholestan-3α-ol (epicoprostanol), plankton origin identified by cholest-5-em-
1172 3β-ol (cholesterol) and 5α-cholestan-3β-ol (cholestanol), and higher plant and algae identified by
1173 24-methylcholesta-5-en-3β-ol(campesterol), 24-ethylcholesta-5,22-dien-3β-ol (stigmasterol) and
1174 24- ethylcholesta-5-en-3β-ol (β-sitosterol). b) Comparison between diagenetic ratio (bars) and
1175 phytosterols concentration (µg $gOrgC^{-1}$ black dots and lines) in upper (U) and lower (L) zone of
1176 Mamanguá (M1), Guapimirim (M2) and Guaratiba (M3) mangroves during summer (S) and winter
1177 periods (W).

1178

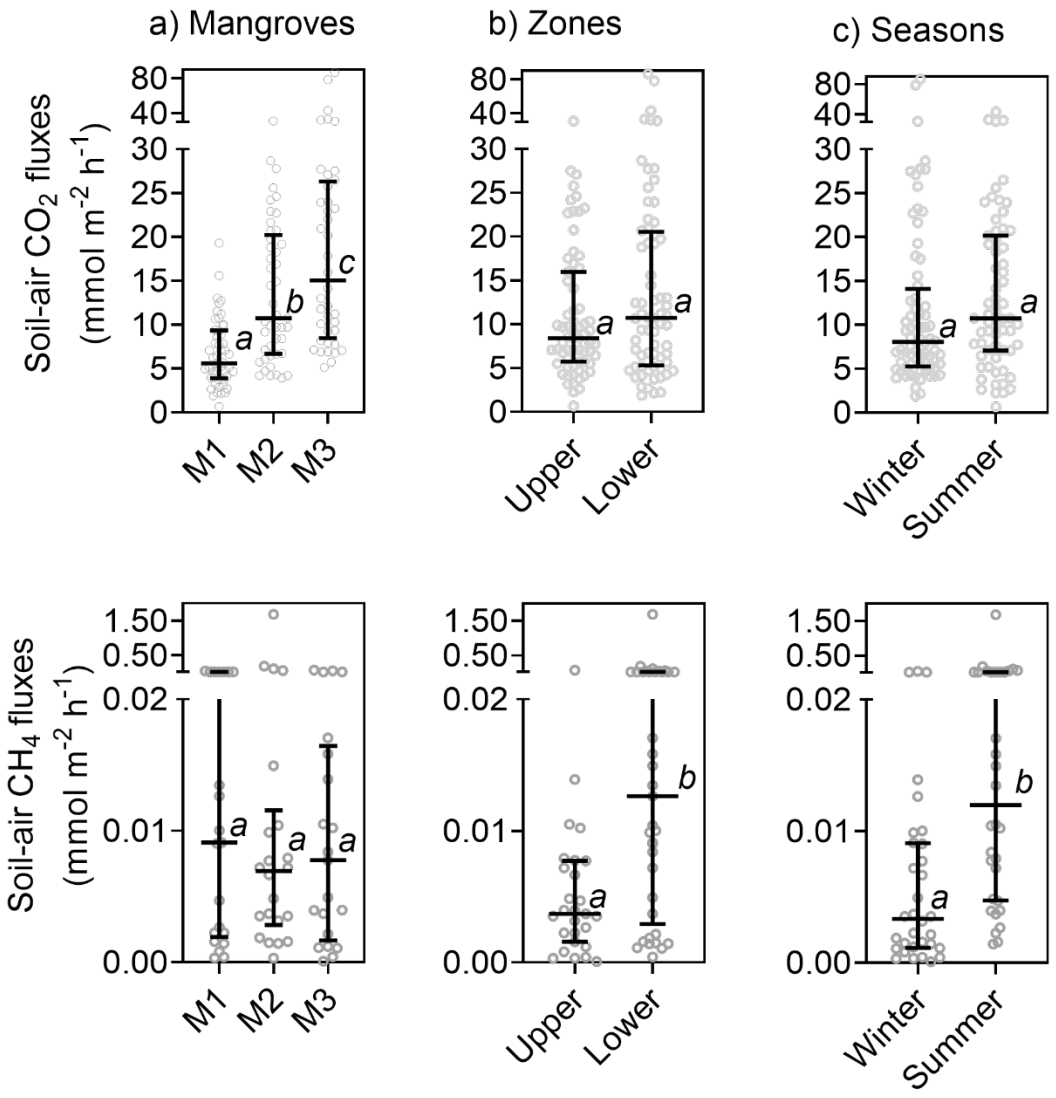

1179

1180 Fig. 5. CO_2 and CH_4 (mmol m^{-2} h^{-1}) fluxes from surface soil to the atmosphere in the upper and
1181 lower zones of Mamanguá (M1) Guapimirim (M2) and Guaratiba (M3) mangroves during summer
1182 and winter periods. Horizontal line represent median, bars represent interquartile range, and
1183 different letters represent statistically significant difference among ecosystems (Kruskal Wallis
1184 Test, p<0,05), intertidal zones and year seasons (Mann-Whitney Test, p<0.05). Clear circles
1185 represent chambers measurements (n=3-5 chambers per zone: season, which were measured 3-7
1186 times consecutively).

1187

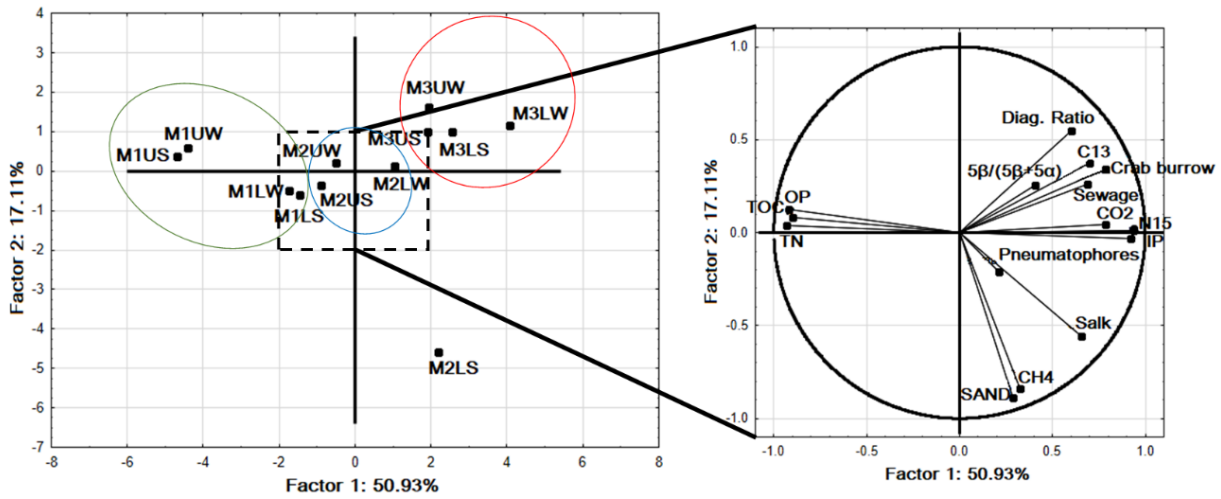

1188

1189 Fig. 6. Principal component analysis showing the magnitude and the direction of correlations
1190 between the different dependent variables: CO_2 and CH_4 fluxes and independent variables: total
1191 organic carbon (OC), total nitrogen (NT), carbon 13 ($\delta^{13}C$), nitrogen 15 ($\delta^{15}N$), diagenetic ratio,
1192 sewage contamination ratio 5β:(5β+5α), sewage presence (coprostanol + epicoprostanol),
1193 inorganic phosphorus (IP), organic phosphorus (OP), sand, and total alkanes (ΣNAlk) in the
1194 mangroves of Mamanguá (M1), Guapimirim (M2), and Guaratiba (M3) according to the two first
1195 axes. The green, blue, and red circles indicate sampling sites from M1, M2, and M3, respectively.

Tables

Table 1. Median (25-75% interquartile range) values of CO_2 (mmol m^{-2} h^{-1}) and CH_4 (μmol m^{-2} h^{-1}) fluxes in the soil-air interface, elementary composition (C, N, P in mg g^{-1}) of surface soil, and number of days of exposed soil conditions in a year in the Mamanguá (M1), Guapimirim (M2), and Guaratiba (M3) mangroves at upper and lower zone during summer and winter period for spring tide.

	Mamanguá (M1)				Guapimirim (M2)				Guaratiba (M3)			
	Upper		Lower		Upper		Lower		Upper		Lower	
	Winter	Summer	Winter	Summer	Winter	Summer	Winter	Summer	Winter	Summer	Winter	Summer
CO_2	5.52 (4.5-7.5)	4.59 (2.9-8.4)	5.0 (3.1-11.2)	8.5 (4.8-10.4)	9.7 (6.1-10.4)	19.5 (16.5-23.9)	6.6 (4.5-23.1)	19.18 (11.6-31.2)	14.8 (6.8-26.1)	8.6 (7.3-13.16)	12.1 (10.5-53.1)	24.0 (21.5-43.1)
CH_4	1 (1-2)	2 (2.5-3)	9 (13-21)	10 (21-23)	3 (4-7)	2 (4-7)	1 (1-7)	8 (39.5-131.5)	1 (2-4)	4 (9-27.5)	1 (2-5)	8 (17-25)
OC	391.8 (370-407)	414.1 (395.9-433.3)	130.9 (110.1-141.1)	115.5 (101.7-162.3)	127.7 (111.9-140)	150.6 (142-160)	79.1 (71-88.3)	67.2 (57.4-82.1)	58.8 (52.2-75.2)	44.7 (38.7-47)	40 (39.3-43.1)	75 (59.4-97.4)
TN	10.6 (10.5-11.1)	11.1 (10.7-11.3)	7.4 (6.9-7.7)	7.9 (6.9-9.2)	6.7 (6.2-7.1)	9.3 (8.9-9.8)	4.7 (4.3-5.1)	4.5 (4.2-5.4)	4.8 (4.2-5.4)	4.1 (3.8-4.3)	4.5 (4.3-4.7)	5.2 (4.7-5.6)
TP	1.23 (1.00-1.8)	1.18 (1.05-1.29)	0.977 (0.92-1.15)	0.86 (0.81-0.92)	1.26 (1.21-1.32)	1.39 (1.35-1.53)	1.14 (1.06-1.19)	1.03 (0.96-1.13)	0.99 (0.96-1.03)	1.13 (1.09-1.16)	1.02 (0.99-1.04)	1.29 (1.21-1.33)
IP	0.09 (0.07-0.13)	0.05 (0.02-0.09)	0.41 (0.28-0.48)	0.32 (0.22-0.46)	0.74 (0.65-0.92)	0.71 (0.69-0.77)	0.84 (0.72-0.99)	0.80 (0.77-0.90)	0.78 (0.74-0.85)	0.77 (0.75-0.84)	0.94 (0.87-0.97)	0.73 (0.67-0.76)

OP	1.21 (0.88-1.72)	1.16 (1.01-1.22)	0.66 (0.49-0.79)	0.54 (0.42-0.59)	0.43 (0.27-0.54)	0.67 (0.59-0.82)	0.31 (0.20-0.38)	0.19 (0.11-0.29)	0.21 (0.15-0.26)	0.33 (0.24-0.37)	0.10 (0.05-0.15)	0.53 (0.42-0.59)
C:N	43.2 (38.5-44.7)	42.6 (41.8-45.6)	20.6 (18.3-21.5)	17.6 (16.7-20.4)	22.3 (21.1-23.8)	18.9 (18.2-19.5)	19.0 (16.9-22.1)	17.1 (15.5-18.2)	14.8 (13.5-16.5)	12.4 (11.1-13.5)	10.6 (9.9-11.7)	16.4 (14.9-21.0)
C:P	301 (221-396)	323 (287-396)	115 (107-143)	139 (121-176)	102 (100-111)	105 (102-111)	73 (68-77)	65 (56-74)	59 (53-76)	40 (37-42)	39 (38-42)	56 (50-78)
$\delta^{15}N$	-0.3 (-1.2-0.9)	0.5 (0-1.4)	2.4 (0.9-3.1)	1.9 (1.7-2.5)	5.2 (5-5.5.4)	3.4 (3-3.5)	6.6 (6.4-7.0)	6.2 (6-6.4)	6.6 (6-7.4)	6.9 (6.5-7.1)	7.0 (6.8-7.4)	5.3 (5.2-5.5)
$\delta^{13}C$	-29.2 (-29.6- -29.1)	-30.3 (-30.6- -29.9)	-24.8 (-25- -24.1)	-25.8 (-25.9- -25.2)	-28,5 (-28.9- -27.7)	-28.4 (-28.6- -28.2)	-27.0 (-27.6- -26.8)	-28.1 (-28.8- -27.8)	-22.9 (-23.7- -22.2)	-22.8 (-24.3- -21.8)	-14.7 (-17.4- -13.3)	-25.7 (-27.1- -22.6)
SAND%	0.1 (0-0.3)	0 (0-52.8)	0	0.1 (0-0.1)	0 (0-0.4)	0 (0-0.3)	5.1 (4.3-36.2)	24.9 (0.2-33.4)	0.2 (0-0.6)	0.1 (0-0.4)	0 (0-0.1)	0.9 (0.4-2.6)
SILT%	86.2 (85.2-88.0)	67.7 (41-69.1)	75.4 (74.9-76.9)	78.8 (77.3-80.1)	87.5 (86.5-89.3)	86.4 (84.6-87.3)	87.4 (57.9-87.9)	66.5 (58.5-86.3)	75.9 (72.2-79.8)	71.1 (63.8-72.6)	81.3 (79.1-82.5)	85.2 (81.1-86.3)
CLAY%	6.7 (5.9-8.3)	15.4 (3.3-16.9)	11.9 (11.5-12.5)	10.5 (10.1-11.4)	7 (5.6-7.6)	7 (6.5-7.9)	4.3 (3.3-4.7)	4.6 (4.2-7.1)	14.2 (11.6-16.2)	17.2 (16.3-21.0)	11.4 (10.4-12.4)	8.2 (6.4-10.9)
OM %	64.8 (63.2-67.0)	73.1 (68.9-73.3)	33.8 (32.2-34.7)	29.7 (28.6-35.2)	32.7 (30.9-34.8)	34.44 (33.82-36.0)	23.2 (21.8-24.5)	18.4 (16.9-21.7)	22.8 (21.3-26.5)	18.7 (17.4-20.2)	19.7 (18.8-20.9)	24.7 (23.5-25.7)

1202 Table 2. Average (±SD) values of $\delta^{13}C$ (‰), $\delta^{15}N$ (‰) and C:N of leaves. stems and roots for the different species in the three studied

1203 mangroves.

		$\delta^{13}C$			$\delta^{15}N$			C:N		
Mangroves	Species	Leaves	Stems	Roots	Leaves	Stems	Roots	Leaves	Stems	Roots
Mamanguá (M1)	*Rhizophora***	-28.4 ± 0.9	-29.2±1.3	-28.7±0.2	1.5±1.0	1.6±0.4	2.6±0.1	32,7±4,8	50,9±1,3	42,2±7,1
	*Avicennia**	-29.9±1.9	-31.5±3.9	-31.2±4.3	2.8±0.9	3.8±2.3	4.2±0.6	35,9±2,3	106,5±66,1	39,6±6,7
Guapimirim (M2)	*Rhizophora***	-28.5 ± 2.9	-28.4±0.7	-30.1±2.2	4.3±0.9	3.8±0.7	4.8±0.4	34,3±1,1	41,8±9,0	35,0±5,6
	*Avicennia**	-32.5±2.1	-29.4±1.9	-29.9±1.8	4.8±0.4	4.8±0.1	5.1±0.2	21,9±3,5	37,6±8,6	36,5±3,3
	*Laguncularia**	-30.4±0.7	-30.2±0.2	-34.6±3.9	6.2±0.9	5.5±0.7	6.4±0.5	27,0±1,3	49,2±8,8	77,7±78,8
Guaratiba (M3)	*Rhizophora***	-28.2 ± 1.6	-27.1±1.9	-28.1±2.7	6.7±0.1	6.2±0.2	6.5±0.2	32,1±5,7	60,1±18,5	69,8±33,5
	*Avicennia**	-32.2±2.9	-31.2±0.9	-33.6±2.5	6.5±0.4	6.4±0.4	7.6±0.3	18,1±5,1	23,5±5,2	119,5±76,3

1204 * Lower Intertidal Zone (Fringe Forest) and **Upper Intertidal Zone (Basin Forest). Mangrove Species: *Avicennia shaueriana*. *Rhizophora*

1205 *mangle* and *Laguncularia racemosa*.

1206

Supplementary Figures

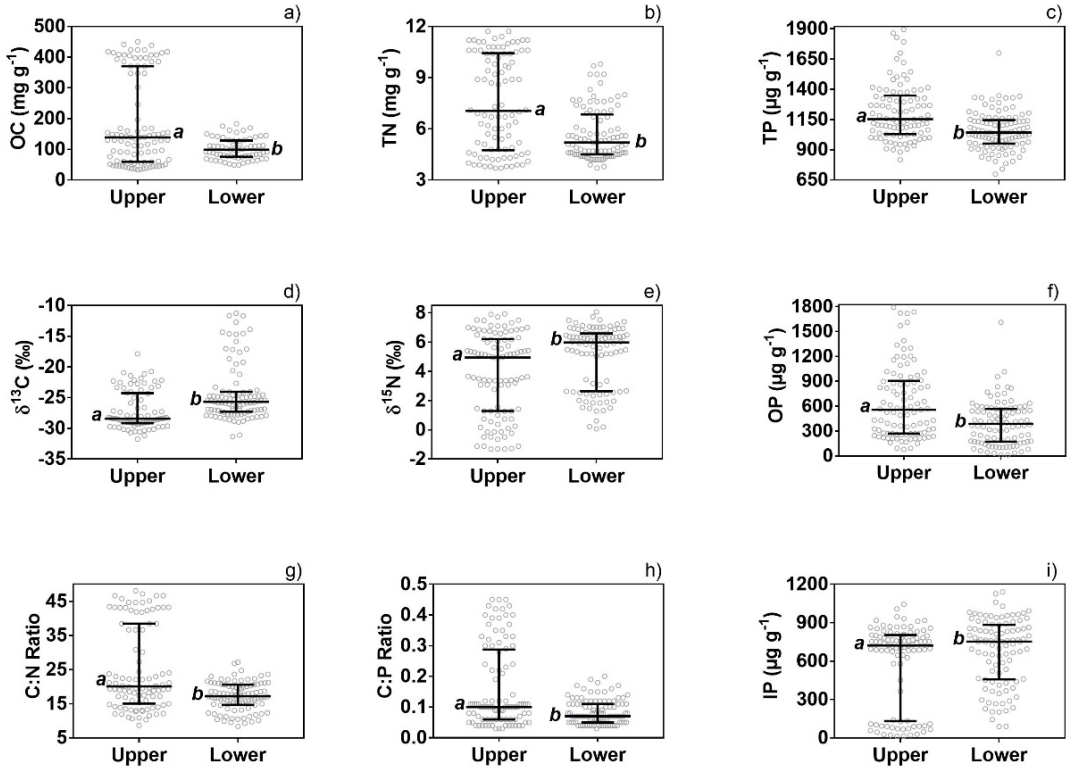

Fig. S1: Intertidal comparison of the elementary composition between upper and lower zones of the studied mangroves soils (Mann-Whitney, $p<0,05$), being a) total organic carbon (OC, mg g^{-1}), b) total nitrogen (TN, mg g^{-1}), c) total phosphorus (TP, µg g^{-1}), d) isotopic ratios of ^{13}C ($\delta^{13}C$, ‰), e) isotopic ratios of ^{15}N ($\delta^{15}N$, ‰), f) organic phosphorus (OP, µg g^{-1}), g) OC to TN ratio (C:N), h) OC to TP ratio (C:P), and i) inorganic phosphorus concentration (IP, µg g^{-1}). Horizontal line represent median, bars represent interquartile range, and different letters represent statistically significant difference.

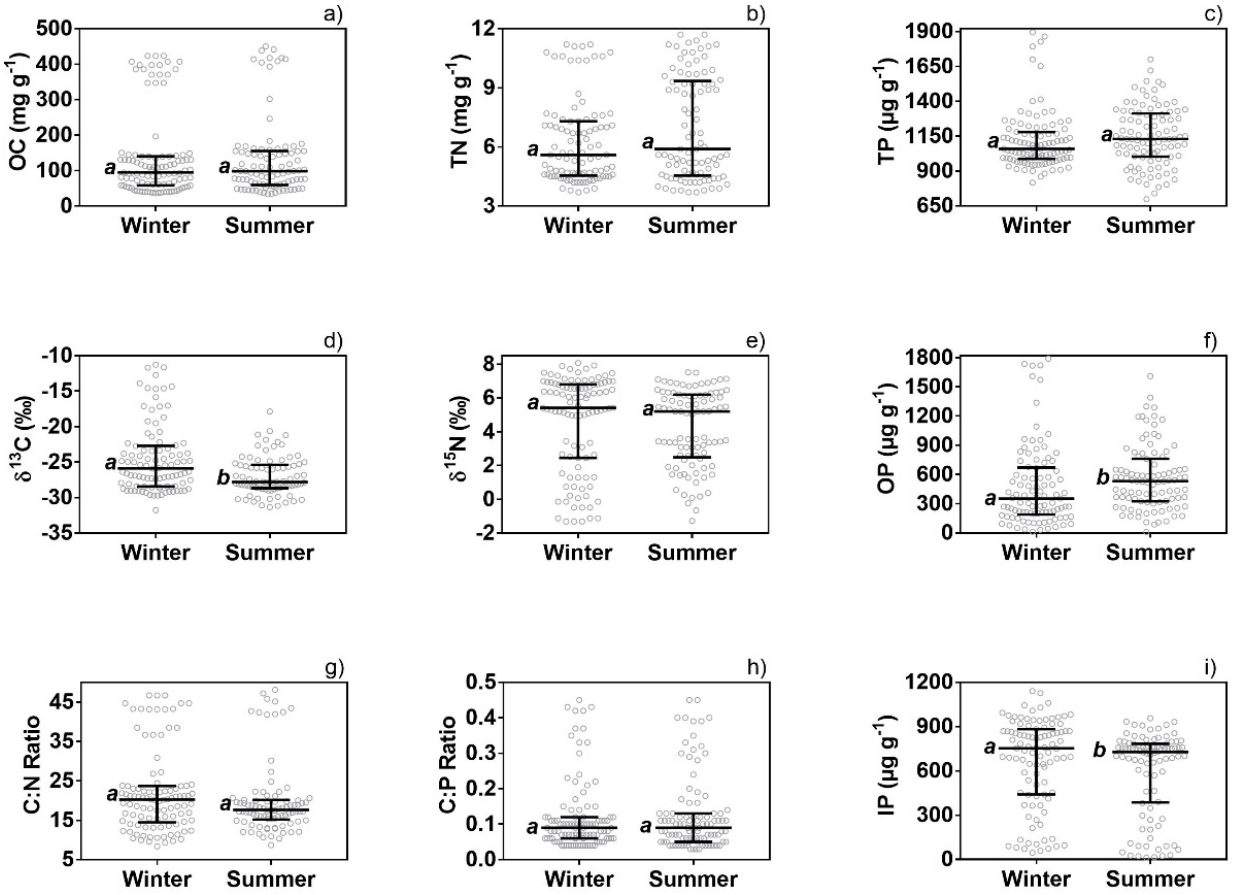

Fig. S2: Seasonal comparison (summer vs. winter) of the elementary composition among the studied mangroves soils (Mann-Whitney, $p<0,05$), being a) total organic carbon (OC, mg g^{-1}), b) total nitrogen (TN, mg g^{-1}), c) total phosphorus (TP, µg g^{-1}), d) isotopic ratios of ^{13}C ($\delta^{13}C$, ‰), e) isotopic ratios of ^{15}N ($\delta^{15}N$, ‰), f) organic phosphorus (OP, µg g^{-1}), g) OC to TN ratio (C:N), h) OC to TP ratio (C:P), and i) inorganic phosphorus concentration (IP, µg g^{-1}). Horizontal line represent median, bars represent interquartile range, and different letters represent statistically significant difference.

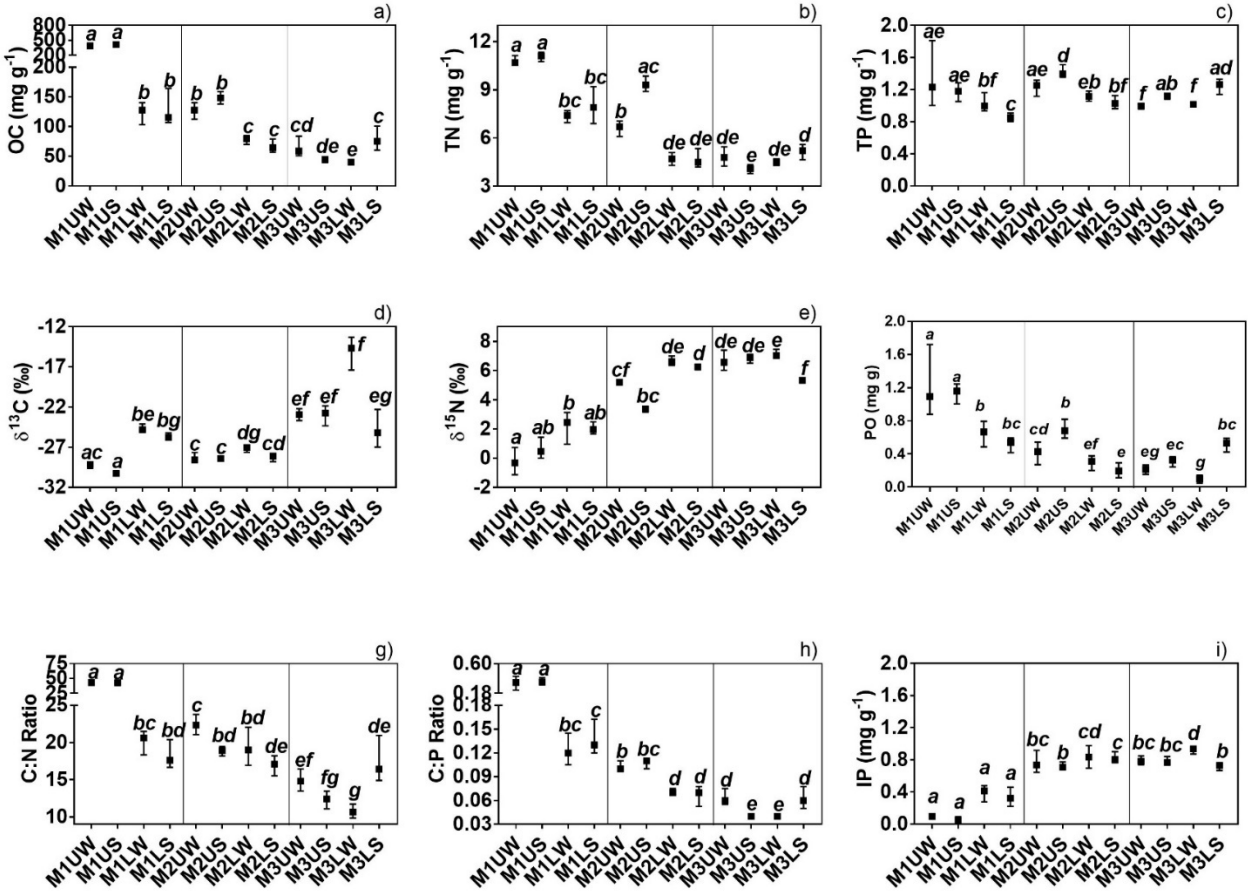

1220

1221 Fig. S3: Spatio-temporal variability among mangroves, zones and seasons for the elementary composition of studied soils, being a) total organic
1222 carbon (OC, mg g^{-1}), b) total nitrogen (TN, mg g^{-1}), c) total phosphorus (TP, mg g^{-1}), d) isotopic ratios of ^{13}C ($\delta^{13}C$, ‰), e) isotopic ratios of ^{15}N
1223 ($\delta^{15}N$, ‰), f) organic phosphorus (OP, mg g^{-1}), g) total organic carbon and total nitrogen ratio (C:N), h) total organic carbon and total phosphorus
1224 ratio (C:P), and i) inorganic phosphorus concentration (IP, mg g^{-1}). Horizontal line represent median, bars represent interquartile range, and different
1225 letters represent statistically significant difference in the Kruskall-Wallis comparison followed by FDR Test ($p<0.05$).

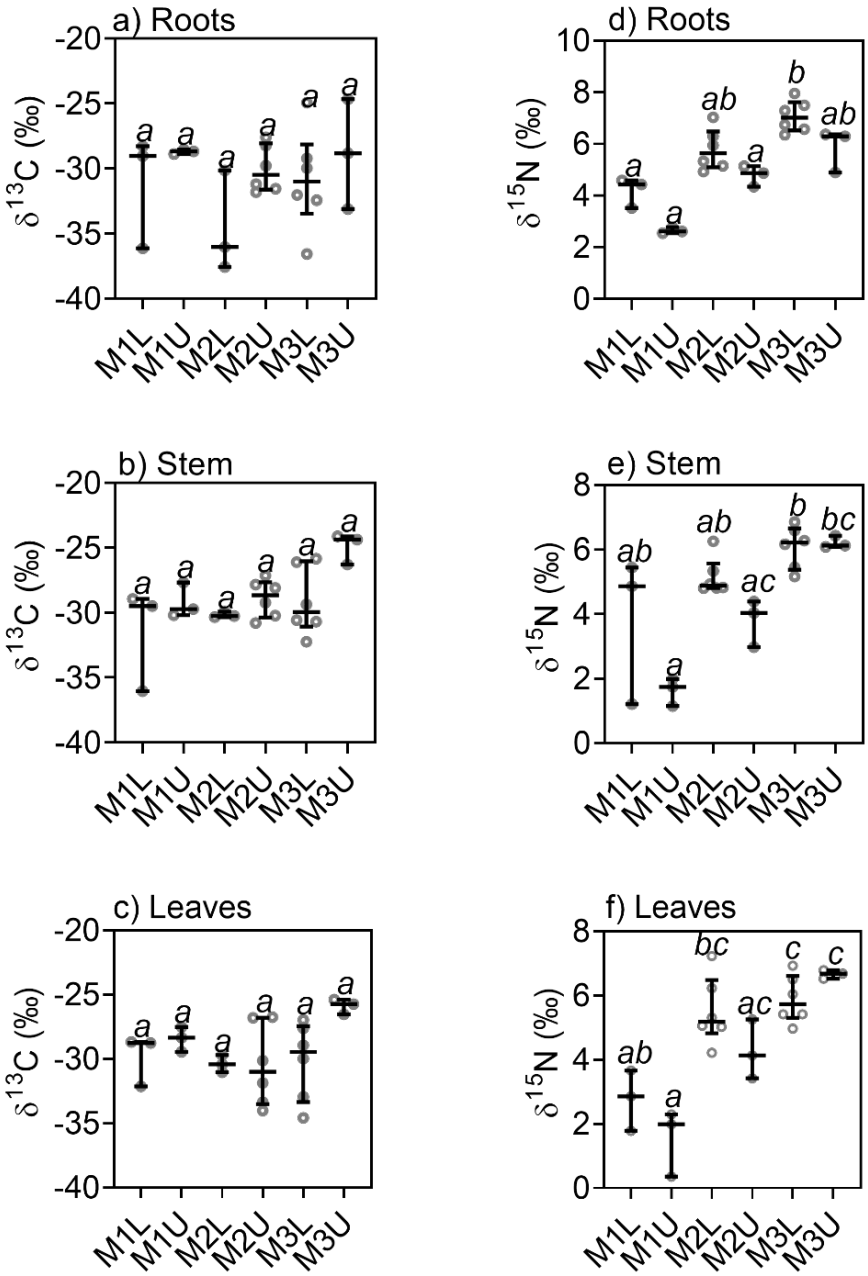

1226

1227 Fig. S4. Comparation of $\delta^{15}N$ and $\delta^{13}C$ from roots, stems, and leaves among upper and
1228 lower zones of Mamanguá (M1), Guapimirim (M2) and Guaratiba (M3) mangroves.
1229 Horizontal line represent median, bars represent interquartile range, and different letters
1230 represent statistically significant difference (Kruskal Wallis followed by FDR post-test;
1231 $p<0.05$).

1232

1233

1234

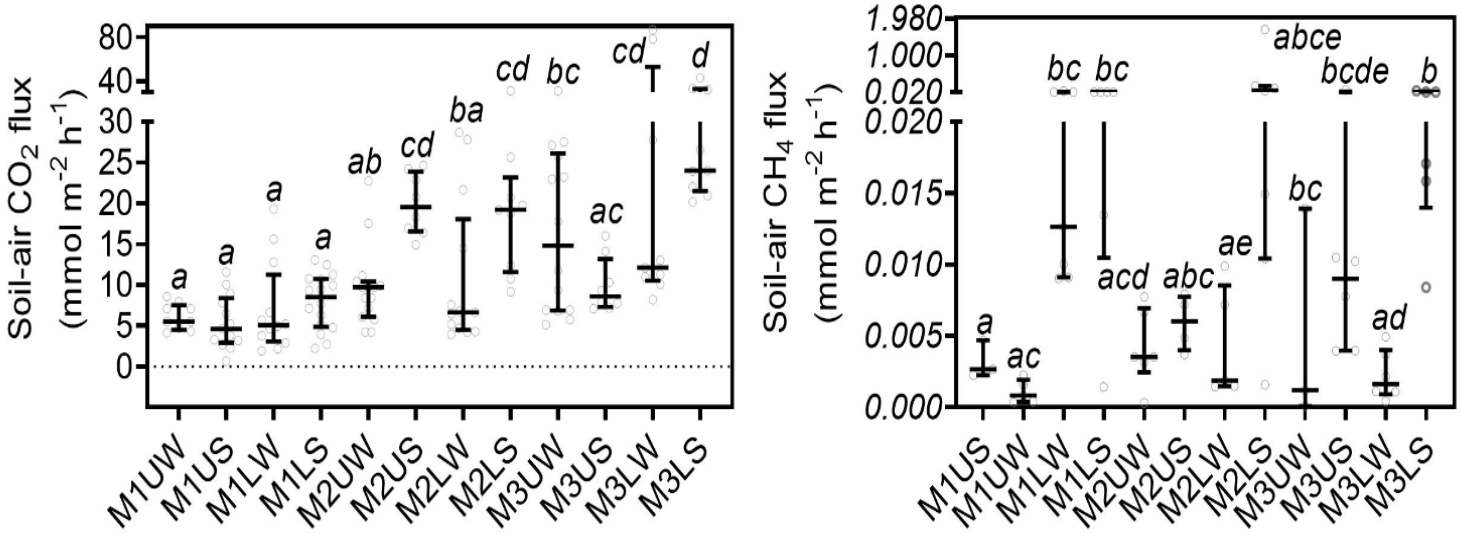

1235 Fig S5: Spatio-temporal variability among mangroves, zones and seasons for the a) CO_2 and b) CH_4 fluxes in the soil-air interface. Horizontal line
1236 represent median, bars represent interquartile range, and different letters represent statistically significant difference in the Analysis of Kruskall-
1237 Wallis followed by FDR test ($p<0.05$). Clear circles represent chambers measurements for CO_2 (n=3-5 chambers per zone: season, which were
1238 measured 3-7 times consecutively) and CH_4 (n=3-7 chambers per zone: season)

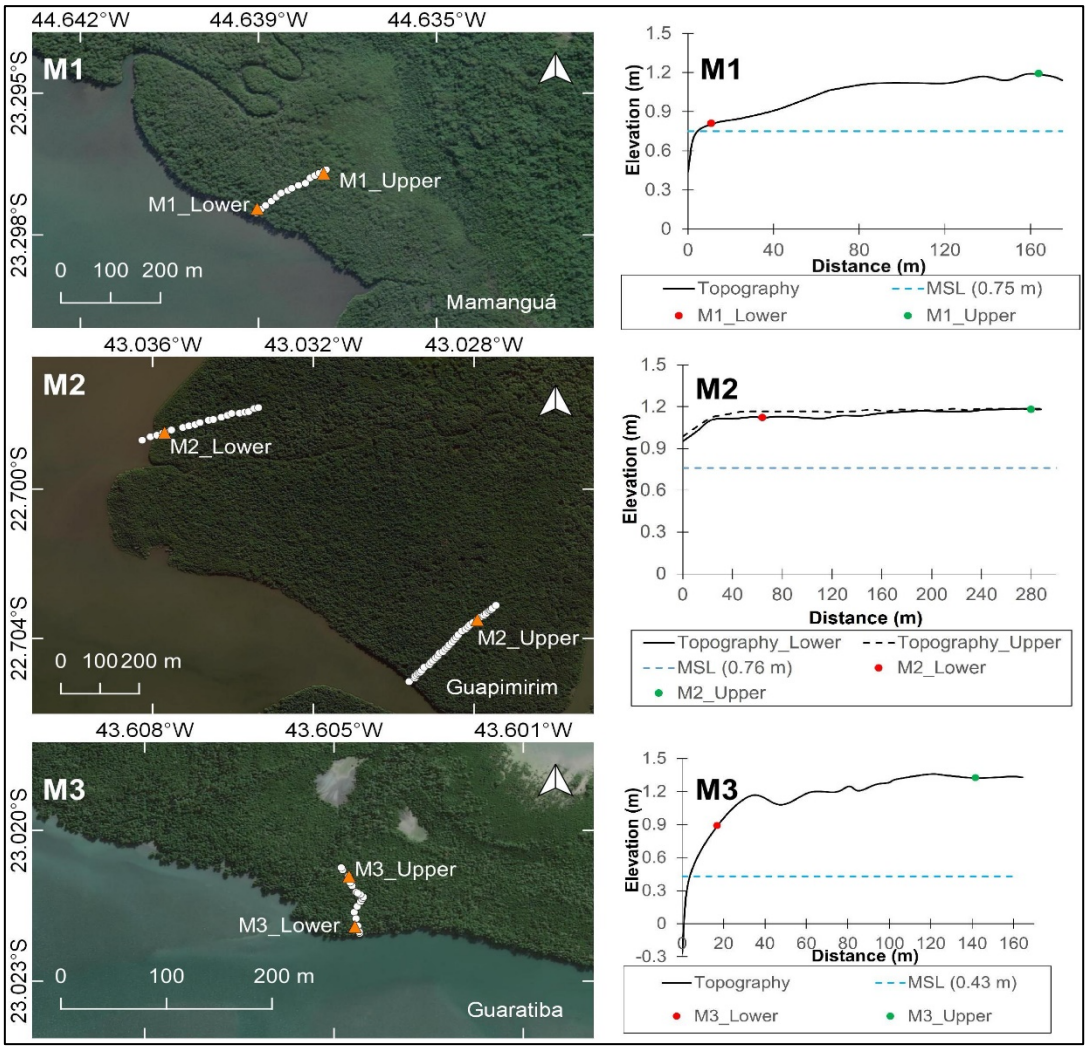

1239

1240 Fig. S6. Topographic profile (white circles) in the study mangroves M1, M2 and M3,
1241 including the sampling points (red triangles) in lower and upper zone. Data calculated
1242 based on the altimetry (Elevation) corrected for the MSL (Mean Sea-Level).

1243

1244

1245

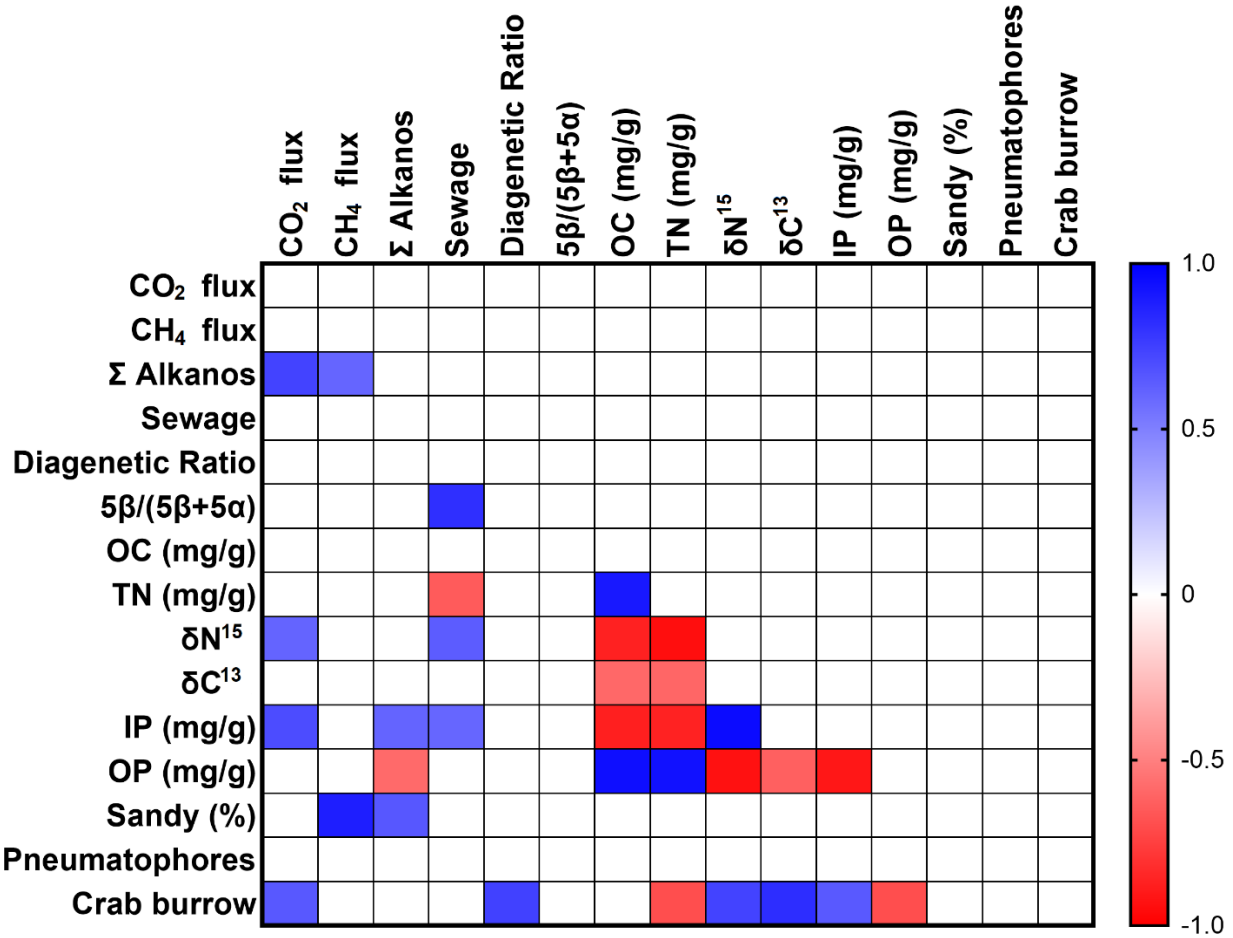

Figure S7: Spearman correlation among soil-air CO_2 and CH_4 flux, Σn-alkanes, Σsterols, diagenetic ratio, 5β:(5β+5α), OC, TN, $\delta^{13}C$, $\delta^{15}N$, IP, OP, sand, pneumatophores and crab burrow. Red squares show significant negative relationships between parameters and blue square show significant positive relationships between parameters ($p<0.05$). Open squares represent show non-significant relationships ($p>0.05$). Each data is the median for each upper or lower zone, mangrove ecosystem, as well as winter or summer (N = 12).

Supplementar Tables

Table S1. Characteristics of the watershed from the studied mangroves areas.

Mangroves	Mamanguá (M1)	Guapimirim (M2)	Guaratiba (M3)
Location	Ilha Grande Bay	Guanabara Bay	Sepetiba Bay
Sampling sites[a]	23°17'48.12"S, 44°38'15.79"O* 23°17'50.80"S;44°38'20.50"O**	22°41'54.55"S,43°2'8.53"O* 22°42'12.60"S.43°1'40.50"O**	23°01'18.99"S,43°36'16.19"O* 23°01'15.28"S;43°36'17.03"O**
Watershead area (Km^2)[b]	17.9	2,078.8	200.8
Approximate Population in the whatershed[c]	2,825	445,610	1,617,538
Population density of the municipality (Hab/Km^2)[c]	158	215	8,056
Dominant land use[d] (%)			
Urban	0.0	3.8	27.8
Fields	0.7	54.4	33.9
Upward Forest	91.8	40.4	30.8
Mangroves	7.5	1.3	6.0
Water	0.0	0.1	0.1
Others[e]	0.0	0.1	1.3
Level of modification	Relatively pristine	Modified	Extensively modified
Dominant mangroves species	*A. shaueriana*, R. mangle***	*L. racemosa*, R. mangle***	*A. shaueriana*, R. mangle*, ***

[a] Mangrove Forest.

[b] Guapimirim, Cachoeira de Macacu and Caceribu sub watershed in M2; and Portinho, Piraquê, Cabuçu and Porto sub watershed in M3.

[c] Data from The Brazilian Institute for Geography and Statistics (IBGE) in 2010 (concerning the approximate population of the districts and villages which each studied watershed).

[d]Land use and land cover was based on the MapBiomas dataset (2017), available at https://plataforma.mapbiomas.org/map#coverage.

[e]Others represent beaches, non-vegetated areas (hilltop, rocky outcrops).

* Lower intertidal zone

**Upper intertidal zone.

Table S2: Physicochemical characteristics of temperature (°C), salinity, DO saturation (%DO, %), dissolved inorganic nitrogen (DIN, uM), and fosfato (PO_4-P, uM) in surface bay waters around Mamanguá (M1), Guapimirim (M2) and Guaratiba (M3) mangroves.

	Mamanguá (M1)		Guapimirim (M2)		Guaratiba (M3)	
	Winter	Summer	Winter	Summer	Winter	Summer
Temperature*	25.7-27.2	30.0-29.0	23.0-22.0	35.3-37.0	24.0-26.0	35.4-30.8
Salinity*	30.4-32.0	31.6-32.6	25.0-22.6	20.0-21.3	29.0-29.0	23.7-27.3
% DO*	78.7-63.7	60.0-69.3	78.7-54.7	58.8-62.0	138.9-57.0	210.0-51.4
DIN**	0.5-0.5	1.1-13.5	14.4-17.6	26.1-37.4	no data	20.6-86.9
PO_4-P**	0.9-1.2	1.2-1.4	0.7-0.8	1.6-1.8	no data	1.5-2.7

* Temperature and %DO were taken using a YSI Pro ODO thermoximeter, while salinity by a WTW Cond 330i conductivimeter.

** DIN as the sum of NH_4-N, NO_2-N, and NO_3-N, as well as PO_4-P were determined by standard methods (APHA et al., 2012) using a Hach DR/4000 spectrophotometer.

Table S3: Molecular composition (Total organic carbon (OC, g g^{-1})), sterol (µg $gOrgC^{-1}$), and ∑n-alkanes (µg g^{-1}) concentrations, as well as diagnostic ratio in surface soils in the Mamanguá (M1), Guapimirim (M2), and Guaratiba (M3) mangroves at upper and lower zone during summer and winter period for spring tide.

	Mamanguá (M1)				Guapimirim (M2)				Guaratiba (M3)			
	Upper		Lower		Upper		Lower		Upper		Lower	
	Winter	Sumer	Winter	Sumer	Winter	Summer	Winter	Summer	Winter	Summer	Winter	Summer
OC	0.39	0.41	0.13	0.12	0.13	0.15	0.08	0.06	0.06	0.04	0.04	0.08
Coprostanol	0.88	0.29	<DL	1.71	1.57	1.09	4.45	3.22	0.95	1.01	3.55	5.08
Epicoprostanol	0.49	<DL	<DL	0.87	<DL	2.62	4.84	<DL	1.89	8.00	3.00	6.52
Cholesterol	6.65	4.02	14.61	51.78	10.60	13.87	55.24	46.80	2.15	9.17	21.25	3.32
Cholestanol	3.71	3.43	4.69	16.07	6.74	7.79	14.03	22.04	21.75	2.80	13.55	2.81
Campesterol	15.85	26.46	11.11	52.51	23.34	26.99	70.87	89.68	9.53	16.88	29.62	7.67
Campestanol	10.10	14.59	17.30	30.86	11.72	21.36	67.60	56.74	51.68	104.51	94.82	52.66
Stigmasterol	61.15	101.58	38.49	265.04	69.50	86.40	182.87	341.91	7.22	26.46	42.64	12.01
Stigmastanol	13.09	23.62	9.61	35.33	11.22	14.79	54.65	57.36	3.57	5.15	13.85	2.70
β-Sitosterol	75.08	138.57	28.22	240.98	121.54	146.10	156.98	386.47	7.25	27.06	17.48	8.26
β-Sitostanol	15.50	28.45	6.15	29.42	15.49	20.34	34.24	65.78	12.44	3.37	11.19	2.62
Total Sterols	202.50	341.00	130.18	724.56	271.73	341.35	645.75	1,070.00	118.44	204.41	250.94	103.65
Phytosterol	152.08	266.61	77.83	558.52	214.39	259.49	410.72	818.06	24.00	70.39	89.74	27.94
Diagenetic Ratio	0.25	0.25	0.42	0.17	0.18	0.22	0.38	0.22	2.82	1.61	1.34	2.08
5β:(5β+5α)	0.19	0.08	<DL	0.10	0.19	0.12	0.24	0.13	0.04	0.27	0.21	0.64
Cop:Cho	0.13	0.07	<DL	0.03	0.15	0.08	0.08	0.07	0.44	0.11	0.17	1.53
∑n-alkanes	186.30	242.60	444.10	1066.80	743.40	2327.30	1010.50	4021.1	693.10	1129.40	3287.2	1655.80
LMW:HMW	0.28	0.22	0.34	0.25	0.21	0.18	0.18	0.15	0.45	0.51	0.22	0.07
CPI	4.10	2.40	4.0	4.80	2.70	4.00	2.90	1.60	2.20	2.00	1.30	2.90
TAR	31.80	33.30	19.9	19.70	24.60	13.40	39.70	15.10	5.10	3.90	20.3	53.5
Pr:Ph	0.30	0.30	0.40	0.60	0.20	0.40	0.20	0.30	0.40	0.20	0.60	0.40
Odd:Even	4.10	2.40	3.90	4.80	2.70	4.00	2.90	1.60	2.20	2.00	1.30	2.90

Phytosterol includes campesterol. stigmasterol. and β-sitosterol. Diagenetic ratio calculated as ∑n-stanol:∑n-sterol. 5β:(5β+5α) calculated as coprostanol:(coprostanol+cholestanol). Cop:Cho calculated as coprostanol:cholesterol. CPI: Carbon preferential index considering Cn_{12-38}. LMH:HMW calculated as ∑short chain (C_{14-23}): ∑long chain (C_{24-40}). TAR (Terrestrial:Aquatic ratio) calculated as ∑ (C_{27}; C_{29}; C_{31}) :∑ (C_{15}; C_{17}; C_{19}). Pr: Ph = pristano:phytano. All data normalized by OC concentration in the soil (for original data in µg g^{-1} see Fig. S3).

Table S4. Total organic carbon (OC g g^{-1}) and sterols concentrations (µg g^{-1}). ∑n-alcanos (µg g^{-1}), diagenetic ratio. 5β:(5β+5α), and Cop: Cho in upper and lower zone of Mamanguá (M1). Guapimirim (M2) and Guaratiba (M3) mangroves during winter and summer periods. Data used to calculate standardize values reported in table S3 in µg $gCOrg^{-1}$.

	Mamanguá (M1)				Guapimirim (M2)				Guaratiba (M3)			
	Upper		Lower		Upper		Lower		Upper		Lower	
	Winter	Sumer	Winter	Sumer	Winter	Summer	Winter	Summer	Winter	Summer	Winter	Summer
OC	0.39	0.41	0.13	0.12	0.13	0.15	0.08	0.06	0.06	0.04	0.04	0.08
Coprostanol	0.35	0.12	<DL	0.20	0.20	0.16	0.35	0.21	0.06	0.05	0.14	0.38
Epicoprostanol	0.19	<DL	<DL	0.10	<DL	0.39	0.38	<DL	0.11	0.36	0.12	0.49
Cholesterol	2.61	1.67	1.87	5.98	1.35	2.06	4.37	3.02	0.13	0.41	0.86	0.25
Cholestanol	1.45	1.42	0.60	1.86	0.86	1.16	1.11	1.42	1.28	0.13	0.55	0.21
Campesterol	6.21	10.96	1.42	6.06	2.98	4.00	5.61	5.79	0.56	0.75	1.19	0.58
Campestanol	3.96	6.04	2.21	3.56	1.50	3.17	5.35	3.66	3.04	4.67	3.82	3.97
Stigmasterol	23.96	42.06	4.91	30.61	8.88	12.81	14.47	22.07	0.42	1.18	1.72	0.91
Stigmastanol	5.13	9.78	1.23	4.08	1.43	2.19	4.32	3.70	0.21	0.23	0.56	0.2
β-Sitosterol	29.42	57.38	3.60	27.83	15.52	21.67	12.42	24.95	0.43	1.21	0.7	0.62
β-Sitostanol	6.07	11.78	0.79	3.40	1.98	3.02	2.71	4.25	0.73	0.15	0.45	0.2
Total Sterols	79.34	141.21	16.61	83.69	34.70	50.62	51.08	69.07	6.96	9.14	10.11	7.81
Phytosterol	59.58	110.40	9.93	64.51	27.38	38.48	32.49	52.81	1.41	3.15	3.62	2.11
Diagenetic Ratio	0.42	0.17	0.25	0.25	0.38	0.22	0.18	0.22	1.34	2.08	2.82	1.61
5β:(5β+5α)	0.20	0.10	<DL	0.10	0.20	0.10	0.20	0.10	0.60	<DL	0.10	0.2
Cop:Cho	0.10	0.10	<DL	<DL	0.10	0.10	0.10	0.10	1.50	0.40	0.10	0.2
∑n-alkanes	73.9	101.60	58.50	125.50	96.60	350.70	81.20	264.00	43.10	55.20	134.20	125.40
LMW:HMW	0.30	0.20	0.40	0.30	0.20	0.20	0.20	0.20	0.50	0.70	0.20	0.10
CPI	4.10	2.40	3.90	4.80	2.70	4.00	2.90	1.60	2.20	2.00	1.30	2.90
RTA	31.80	33.30	19.90	19.70	24.6	13.40	39.70	15.10	5.10	3.90	20.30	53.50
Pr:Ph	0.30	0.30	0.40	0.60	0.20	0.40	0.20	0.30	0.40	0.20	0.60	0.40
Odd:Even	4.10	2.40	3.90	4.80	2.70	4.00	2.90	1.60	2.20	2.00	1.30	2.90

1291 Legenda: Phytosterol includes campesterol. stigmasterol. and β-sitosterol. Diagenetic ratio calculated as ∑n-stanol:∑n-sterol. 5β:(5β+5α)
1292 calculated as coprostanol:(coprostanol+cholestanol). Cop:Cho calculated as coprostanol: cholesterol. CPI: Carbon preferential index considering
1293 Cn_{12-38}. LMH:HMW calculated as ∑short chain (C_{14-23}):∑long chain (C_{24-40}). TAR (Terrestrial:Aquatic ratio) calculated as ∑ (C_{27}; C_{29}; C_{31}) :∑
1294 (C_{15}; C_{17}; C_{19}). Pr:Ph = pristano:phytano.
1295
1296
1297
1298
1299
1300
1301
1302
1303

Table S5. Concentration of n-alkanes from C-14 to C-40 chain (μg g^{-1}) in surface soil of lower (L) and upper(U) zone from Mamanguá (M1). Guapimirim (M2) and Guaratiba (M3) mangroves during winter (W) and summer (S) periods.

	Mamanguá (M1)				Guapimirim (M2)				Guaratipa (M3)			
	Upper		Lower		Upper		Lower		Upper		Lower	
	Winter	Summer	Winter	Summer	Winter	Summer	Winter	Summer	Winter	Summer	Winter	Summer
C14	0.12	0.19	0.10	0.47	0.13	4.20	0.09	1.55	0.19	0.49	0.16	0.51
C15	0.12	0.16	<LD	0.58	0.16	7.02	0.11	3.86	0.64	1.23	0.19	0.54
C16	0.12	0.13	0.39	1.28	0.34	4.98	0.19	3.60	0.78	1.42	0.69	0.67
C17	0.22	0.25	0.51	1.25	0.55	3.94	0.24	1.85	1.01	1.58	0.88	0.33
C18	0.95	0.48	1.10	1.73	0.38	1.57	0.85	1.25	0.74	1.86	0.48	0.19
C19	0.54	0.64	0.55	0.94	0.76	2.51	0.58	0.89	0.72	0.82	0.76	0.14
C20	1.11	0.92	1.33	0.99	0.85	2.35	0.89	1.56	0.91	1.69	0.70	0.22
C21	2.52	2.70	2.07	3.24	2.52	5.74	2.59	3.36	2.98	3.08	10.87	2.33
C22	0.65	1.77	0.83	1.72	1.56	2.66	1.13	3.36	0.90	0.95	2.27	<LD
C23	9.41	10.81	7.39	12.19	8.96	18.80	5.71	13.40	3.80	3.88	7.04	3.05
C24	3.99	7.96	1.96	3.30	5.14	11.89	3.05	17.76	1.66	1.57	9.53	1.28
C25	17.33	19.87	12.28	24.53	18.41	45.24	10.62	33.29	5.04	7.18	15.67	7.05
C26	2.65	6.84	1.43	2.37	6.21	6.49	4.13	26.67	1.00	2.56	16.72	1.80
C27	11.29	14.97	7.18	18.54	15.13	54.71	12.20	43.39	4.45	4.72	18.10	8.76
C28	3.06	6.66	2.00	4.59	5.92	16.54	5.24	25.55	3.07	2.99	15.41	3.75
C29	14.58	16.58	9.77	24.60	15.26	83.98	19.95	45.40	5.11	5.57	13.31	19.11
C30	1.40	3.15	1.39	3.09	3.48	13.61	3.25	12.37	2.40	2.12	8.05	7.99
C31	2.05	3.24	4.15	11.31	5.89	41.84	4.40	10.68	2.58	3.72	5.56	26.69
C32	0.27	0.93	0.36	1.38	0.95	3.47	1.03	4.26	0.61	0.81	2.98	5.51
C33	0.43	0.97	1.29	4.24	1.49	11.23	2.41	3.36	1.20	1.47	2.01	15.73
C34	0.09	0.19	0.11	0.48	0.25	0.85	0.43	0.79	0.34	0.31	0.71	4.79
C35	0.11	0.29	0.22	0.40	0.24	1.39	0.26	0.84	0.31	0.30	0.28	9.22
C36	<LD	0.77	0.25	<LD	0.34	0.15	0.44	0.26	0.32	0.18	0.11	5.11

C37	<LD	<LD	<LD	<LD	<LD	<LD	0.14	0.26	<LD	<LD	<LD	<LD
C38	<LD	<LD	<LD	<LD	<LD	<LD	<LD	<LD	<LD	<LD	<LD	<LD
C39	<LD	<LD	<LD	<LD	<LD	<LD	<LD	<LD	<LD	<LD	<LD	<LD
C40	<LD	<LD	<LD	<LD	<LD	<LD	<LD	<LD	<LD	<LD	<LD	<LD

1319 Table S6: Values of Spearman correlation coefficient (r_s) for statistically significant relationships ($p<0.05$) reported in Fig. S5.

	CO_2 flux	CH_4 flux	Σ Alkanes	Sewage	Diag. Ratio	5ß:(5ß+5a)	OC	TN	δN^{15}	δC^{13}	IP (mg/g)	OP (mg/g)	Sandy (%)	Pneumatophores	Crab burrow
CO_2 flux															
CH_4 flux															
Σ Alkanes	0.74	0.60													
Sewage															
Diag. Ratio															
5ß:(5ß+5a)				0.82											
OC															
TN				-0.64			0.90								
δN^{15}	0.61			0.64			-0.87	-0.95							
δC^{13}							-0.59	-0.60							
IP (mg/g)	0.70		0.60	0.60			-0.88	-0.87	0.96						
OP (mg/g)			-0.59				0.94	0.93	-0.93	-0.63	-0.91				
Sandy (%)		0.88	0.66												
Pneumato-phores															
Crab burrow	0.65				0.74			-0.69	0.73	0.82	0.65	-0.70			

1320

Table S7. Eigenvectors. variables contribution based on correlations from principal component analysis (PCA). factors-variables correlations (factor loadings) based on correlation between variables. Sewage shows coprostanol + epicoprostanol.

	Eigenvectors		Variable contributions		Factor loadings	
	Factor 1	Factor 2	Factor 1	Factor 2	Factor 1	Factor 2
CO_2 flux	0.283877	0.026262	0.080586	0.000690	0.784619	0.042072
CH_4 flux	0.116912	-0.525154	0.013668	0.275787	0.323138	-0.841284
Σ n-Alkanes	0.236693	-0.348214	0.056024	0.121253	0.654206	-0.557831
Sewage	0.248625	0.161782	0.061814	0.026173	0.687184	0.259171
Diagenetic Ratio	0.217566	0.340801	0.047335	0.116145	0.601340	0.545955
5ß/(5ß+5a)	0.146751	0.158754	0.021536	0.025203	0.405611	0.254320
OC	-0.325280	0.049447	0.105807	0.002445	-0.899055	0.079213
TN	-0.337825	0.024001	0.114126	0.000576	-0.933727	0.038448
$\delta^{15}N$	0.340042	0.007945	0.115629	0.000063	0.939856	0.012728
$\delta^{13}C$	0.252864	0.234537	0.063940	0.055008	0.698900	0.375722
IP	0.332472	-0.018883	0.110537	0.000357	0.918931	-0.030250
Sand	-0.333885	-0.076817	0.111479	0.005901	-0.922836	0.123060
OP	0.103943	-0.554104	0.010804	0.307031	0.287292	-0.887661
Pneumatophores	0.077257	-0.133223	0.005969	0.017748	0.213533	-0.213421
Crab burrows	0.284157	0.213590	0.080745	0.045620	0.785393	0.342165